A novel portable oxidation-reduction potential and microbial fuel cell-based sensor to monitor microbial growth

A Thesis Submitted to the

College of Graduate and Postdoctoral Studies

In Partial Fulfillment of the Requirements

For the Degree of

Master of Science

In the Department of Chemical and Biological Engineering
University of Saskatchewan
Saskatoon

By

Peng Teng

PERMISSION TO USE

In presenting this thesis in partial fulfilment of the requirements for a Master of Science degree from the University of Saskatchewan, I agree that the Libraries of this University may make it freely available for inspection. I further agree that permission for copying this thesis, in whole or in part, in any manner for scholarly purposes may be granted by the professor or professors who supervised my thesis work or, in their absence, by the Head of the Department or the Dean of the College in which my thesis work was conducted. It is understood that any copying, publication, or use of this thesis or parts thereof for financial gain shall not be allowed without my written permission. It is also understood that due recognition shall be given to the University of Saskatchewan and me for any scholarly use of any material in my thesis.

Requests for permission to copy or use materials in this thesis/dissertation, in whole or part, should be addressed to:

Head, Department of Chemical and Biological Engineering
University of Saskatchewan
57 Campus Drive
Saskatoon, SK, S7N 5A9,
Canada.

Or the:

Dean, College of Graduate and Postdoctoral Studies
University of Saskatchewan
116 Thorvaldson Building,
110 Science Place Saskatoon, SK, S7N 5C9,
Canada.

ABSTRACT

Bioremediation, the most environment-friendly soil remediation method, should receive adequate attention. However, its efficiency has often been criticized, reflecting the dearth of information about microbial activity in the soil. Biosensors can use the signals sent by microorganisms to quantify and analyze microbial activity. Therefore, combining biosensors with bioremediation can enhance the application of bioremediation technology.

This thesis focused on designing and fabricating of portable microbial fuel cell (MFC) and oxidation-reduction potential (ORP) based sensor to achieve in situ soil bioremediation application in the future. This is because conventional biosensors cannot reflect the detailed microbial growth characteristics during soil bioremediation.

During the experiment, two portable sensors were designed. First, two cylindrical polypropylene bottles were compressed tightly to form a preliminary sensor containing a proton exchange membrane (PEM), an O-ring, and a cathode electrode. After successfully testing the preliminary sensor's workability, a smaller, easier-to-assemble 3D-printed sensor was designed based on the same concept.

The extracellular electrogenic bacterial *Bacillus subtilis* was used to test both sensors' workability. MFC and ORP sensors provide voltage and redox potential outputs. By integrating real-time redox potential and voltage outputs, a typical microbial growth (potential parameter) curve can be created. The derivative optical density (OD) value (OD per hour) was found to correspond to the potential parameter. The preliminary sensor could acquire detailed microbial growth characteristics at 6.5 and 18 hours, and the 3D-printed sensor at 10 and 21 hours. The accompanying derivative OD values supported these conclusions. This novel sensor can monitor real-time microbial growth, report detailed growth characteristics in soil, and help select better bioremediation solutions.

Future work is required to improve the responsive of the 3D-printed sensor to achieve higher-resolution result.

ACKNOWLEDGEMENTS

I would like to express my deep and sincere gratitude to my supervisor, Prof. Yen-Han Lin, for his continuous supervision, positive discussions, insightful advice, patience, and support throughout my study. I owe much of my success to him, and I am grateful to have had the opportunity to learn from his wisdom and experience during my graduate studies.

I would also like to thank the members of my MSc Dissertation Advisory Committee, Prof. Lifeng Zhang and Prof. Amira Abdelrasoul, for their willingness to serve on my committee and their helpful suggestions and feedback about how I could improve my research.

I extend my gratitude to Kevin Carter, Majak Mapiour, RLee Prokopishyn, and Dushmanthi Jayasinghe for their help during my research.

I am also grateful to my colleague, Dr. Qingshan Meng, who educated me with myriad skills and knowledge and patiently answering my questions.

Last but not least, I would like to thank my father, Wenjun Teng, and my mother, Xinlei Guo, for their unconditional love and support and for believing in me, particularly when I found it hard to do so myself. My success would not have been possible without my parents' assistance and support.

TABLE OF CONTENTS

LIST OF FIGURES

NOMENCLATURE

List of Abbreviation

B. subtilis	*Bacillus subtilis*
BFC	Biological fuel cell
BOD	Biochemical oxygen demand
COD	Chemical oxygen demand
HC	Hollow cuboid
LB	Lysogeny broth
MFC	Microbial fuel cell
NAD^+/NADH	Nicotinamide adenine dinucleotide
$NADP^+$/NADPH	Nicotinamide adenine dinucleotide phosphate
OD	Optical density
ORP	Oxygen reduction reaction
PEM	Proton exchange membrane
PLA	Polylactic acid
PP	Polypropylene
RVC	Reticulated vitreous carbon
TSC	Outer shell of three-sided cuboid
UV	Ultraviolet

Roman Symbols

Symbol	Description	Unit
ΔG_r	Gibbs free energy	J mol^{-1}
ΔG_r^0	Standard free energy	J mol^{-1}
R	Universal gas constant	J mol^{-1} K^{-1}

T	Absolute temperature	K
$E_{emf}(E_h)$	Cell electromotive force	mv
Q	Charge transferred	C
$E^0_{emf}(E^0)$	Standard cell electromotive force	mv
n	Electron exchange number	mol
F	Faraday's constant	C mol^{-1}
E_{cell}	Actual electromotive force	mv
I	Current	A
R_Ω	Internal resistance	Ω
vvm	Aeration rate	L L^{-1} min^{-1}
rpm	Rotation speed	r min^{-1}
Red	Reduced state concentration	mol L^{-1}
Ox	Oxidized state concentration	mol L^{-1}
C	Reference potential	mv

Greek Symbols

Symbol	**Description**	**Unit**
Π	Reaction quotient	N/A
$\sum\eta_a$	Anode overpotentials	mv
$\lvert\sum\eta_c\rvert$	Cathode overpotenti	

1 INTRODUCTION

1.1 Problem Definition

Anthropogenic pressure and excessive land development will create serious soil contaminants (Ashraf et al., 2014). As an essential resource, the soil has a close relationship with people's daily lives. The ground can be physically used for city construction, as a buffer for groundwater cleaning, and as agriculture or pasture (Van Straalen, 2002). The bioremediation method can be a suitable choice for this problem because it is cheap, can maintain soil structure, and is environmentally friendly (Jin, 2018). However, because the bioremediation treatment happened underneath, the appropriate microbial activity was hard to identify (Vishwakarma et al., 2020; Patel et al., 2020). Monitoring microbial activity in soil is essential to enhance the application of bioremediation technology.

Biosensors recently gained attention because of their relatively simple operation and low cost (Justino et al., 2017). A biosensor can directly detect the reaction between biological compounds and pollutants in the soil and convert the signal sent by microorganisms into a readable digital signal (Shukla et al., 2018). Therefore, through real-time information reporting, the user could intuitively and quickly understand the microorganisms' status and whether the selected biodegradation method has performed its function in the soil (Dennison & Turner, 1995).

1.2 Research Background

1.2.1 Oxidation-Reduction Potential

An oxidation-reduction potential (ORP) sensor uses electrochemical transduction with a working electrode generating potential and a reference electrode contributing constant voltage (Kruse et al., 2018; Steininger & Pareja, 1996). The ORP value can reflect water and biological process quality by detecting oxidant and reductant amounts (Copeland & Lytle, 2014). The more oxidants in the

water, the healthier it is. The more reductants in the water, the more polluted it is with organic and inorganic contaminants (Steininger & Pareja, 1996; Copeland & Lytle, 2014). ORP sensors can also reflect the bioreactor's real-time metabolic activity by detecting extracellular oxygen and substrate consumption during fermentation (Liu et al., 2012; Liu et al., 2017). Therefore, metabolites such as pickles, yogurt, beer, and ethanol can all be influenced by controlling the ORP value (Liu et al., 2012). Monitoring the entire fermentation process with an ORP sensor showed a close relationship between the ORP value and microbial growth (Liu et al., 2017). Therefore, the ORP value could also reflect general microbial growth. Because microbial activity mainly controls the entire redox process in the earth, the growth rate of microorganisms in the soil could be reflected in the redox potential reported by an ORP sensor (Fiedler et al., 2007).

1.2.2 Microbial Fuel Cell

Since 2007, research on using microbial fuel cell (MFC) devices as biosensors has received much attention (Zhou et al., 2017). An MFC device could achieve sustainability, cost-effectiveness, design simplicity, and remote monitoring as a natural environment sensor (El Mekawy et al., 2018). As a bioelectrochemical reactor, the MFC uses anaerobic or microaerobic bacteria to oxidize organic or inorganic compounds to produce electrons. The biofilm and suspended bacteria help the released electrons transfer from the anode to the cathode through an external wire in the anode compartment. Water can form in the cathode compartment by combining the transferred electrons with oxygen from the environment and protons from the anode compartment through a proton exchange membrane (PEM; Beecroft, 2010; Rahimnejad et al., 2015). The difference between the cathode and anode potential creates the voltage. Through total electron production, MFC devices could act as power collectors or sensors to detect microbial activity (Logan et al., 2006). Most MFC devices can be classified as single-chamber or double-chamber (Tamboli & Eswari, 2019). Single-chamber MFC devices are more suitable for biosensors because of their better sensitivity, operability, and compactness than dual-chamber MFC devices (Zhou et al., 2017).

1.3 Thesis Organization

This project's overall goal was to design a novel miniature MFC and ORP to monitor the real-time microbial growth rate and provide in-depth information. Chapter 1 describes the relationship between soil contamination, bioremediation, and biosensors and briefly explained ORP and MFC biosensors. Chapter 2 describes the background knowledge, fabrication, configuration, and

application of MFC and ORP sensors. Chapter 3 lists all the materials and design methods used to fabricate the preliminary and 3D-printed sensor. It also explains the specific bacterial strain and experimental setup. Data analyses methods and devices are mentioned in the end. Chapter 4 illustrates the workability of the preliminary and 3D-printed sensors by integrating the redox potential and voltage output into the modified Nernst equation, measuring the optical density (OD) of solution samples, and plotting the graphs. Chapter 5 concludes this thesis by describing the preliminary and 3D-printed sensors' final results to demonstrate their workability. Furthermore, several suggestions will be provided for improving this portable sensor's performance. Finally, all the references and appendices are included in the end of the article.

2 LITERATURE REVIEW

2.1 ORP Sensor Overview

2.1.1 ORP Sensor Composition

An ORP sensor comprises a reference and a measuring system. The reference system comprises a silver wire, silver chloride coating, and saturated potassium chloride solution. It should have a stable voltage output based on Nernst's law. The measuring system comprises a noble metal (platinum) wire because it will not interfere with the chemical reaction in the solution (Yokogawa, 2014).

2.1.2 Working Principle of an ORP Sensor

Theoretically, the ORP reflects the tendency for molecules to lose or accept electrons during a reaction (Brundage, 2021). During electron transfer, the oxidizing agent accepts electrons, and the reducing agent donates electrons (James et al., 2004). Therefore, the redox reaction can be divided into two half-reactions. Common examples in chemistry are iodide losing two electrons to become iodine and a ferric ion receiving two electrons to form a ferrous ion (Liu et al., 2017).

$$\text{Oxidation: } 2I^- = I_2 + 2e^- \quad (2.1)$$

$$\text{Reduction: } 2Fe^{3+} + 2e^- = 2Fe^{2+} \quad (2.2)$$

$$\text{Redox reaction: } 2Fe^{3+} + 2I^- = 2Fe^{2+} + I_2 \quad (2.3)$$

Each half-reaction has a standard redox potential value at 25°C (Yokogawa, 2014). However, in actual measurements, environmental conditions always differ from the standard, causing variable redox potentials (Brundage, 2021). Therefore, Walther Heman Nernst developed a Nernst equation

to relate the standard redox potential value to the surrounding environmental conditions (Liu et al., 2017).

Nernst formula:

$$E_h = E^0 - \frac{RT}{nF} ln \frac{[Red]}{[Ox]} \quad (2.4)$$

- E_h = real-world redox potential (mv)
- E^0 = standard potential (mv)
- R = universal gas constant (8.314 J mol^{-1} K^{-1})
- T = temperature (K)
- n = number of transferred electrons
- F = Faraday's constant (96,500 C mol^{-1})
- Red = reduced state concentration (mol L^{-1})
- Ox = oxidized state concentration (mol L^{-1})

The ORP sensor measures all redox reactions in a sample ($E_{measured}$; Liu et al., 2017; James et al., 2004). The platinum electrode measures the sample's oxidizing or reducing tendency as the difference in free electrons between the two half-reactions (E_h; Crofts, 1996; James et al., 2004). A reference potential (Ag/AgCl) is used (C) to relate the sample's measured potential to the redox potential (James et al., 2004).

$$E_h = E_{meaured} + C \quad (2.5)$$

2.1.3 Application

The ORP value is a chemical parameter indicative of water quality (Kruse, 2018) because its fluctuation can reflect the water's oxidation or reduction tendency. In healthy water, it is determined by oxidants such as iron, chlorine, and oxygen (Copeland & Lyrle, 2014). Reducers such as oil, urea, and bacteria can greatly influence water quality (Steininger & Pareja, 1996). Furthermore, ORP sensors applied to drinking, waste, swimming pool, and industrial water can reflect sanitizer concentrations (Kruse, 2018; Steininger & Pareja, 1996). Common disinfectants, such as chlorine dioxide, dissolved oxygen, and potassium permanganate, can be detected by ORP sensors. Therefore, the ORP sensor can also assess sanitizer efficiency. The applied disinfectants'

concentration should reach a specific ORP value to kill microorganisms better (Copeland & Lyrle, 2014).

The redox potential value also applies to the living cell (Needham & Needham, 1926). A cell's redox potential reflects total electron transfer and redox balance during intracellular metabolism (Liu, 2012). Maintaining intracellular redox balance during metabolism is necessary for regular cellular function (Foyer & Noctor, 2005). Unreduced $NAD(P)^+$ and reduced NAD(P)H nicotinamide adenine dinucleotide phosphate are the primary redox pair maintaining the intracellular redox balance (Liu, 2017). During catabolism, the coenzyme nicotinamide adenine dinucleotide NAD^+ accepts electrons from other molecules to form NADH and reduced substrates. During anabolism, the major cofactor $NADP^+$ accepts electrons to form NADPH and achieve biosynthesis (Liu et al., 2012; Liu et al., 2017). To balance the intracellular redox potential, oxidants such as oxygen, hydrogen peroxide, and dithiothreitol enter the cytoplasm to reoxidize NADPH (Liu et al., 2017; de Graef et al., 1999). The internal steady-state $NADP^+$ to NADPH ratio mainly relies on the nature of external electron acceptors (de Graef et al., 1999). Therefore, the ORP sensor detects the environmental oxidation-reduction tendency to reflect intracellular metabolism (Figure 2.1).

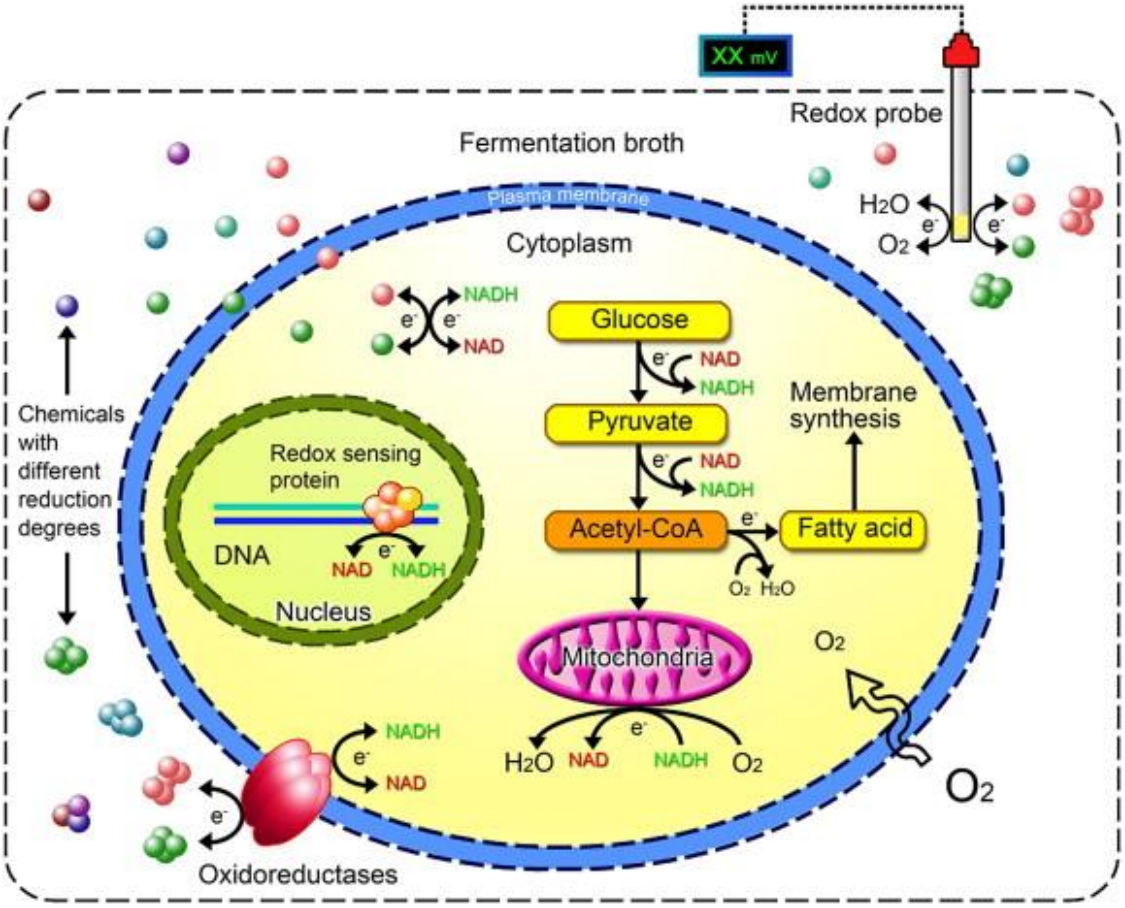

FIGURE 2.1 The relationship between the environmental redox potential and intracellular metabolism. The figure is reproduced from Liu et al. (2012). (Permission to reproduce is granted by Elsevier)

Generally, monitoring the microorganism metabolism can reflect fermentation, substrate uptake and utilization (inorganic or organic compounds), and cell growth (Jurtshuk, 1996; Najafpour, 2007). Furthermore, monitoring the entire fermentation process with an ORP sensor showed a close relationship between ORP values and microbial growth (Liu et al., 2017). Therefore, ORP sensor monitoring can directly detect the microbial growth rate. Because microbial activity mainly controls the entire redox process in the earth, electron transfer during intracellular metabolic processes and microbial growth rate in the soil can be monitored via the redox potential detected by the ORP sensor (Fiedler et al., 2007; Liu et al., 2017).

Changes in environmental conditions can alter the expression of genes encoding specific enzymes. The in vivo flux of NADH-dependent enzymes is influenced by extracellular electron acceptor

availability (de Graef et al., 1999). Therefore, the overexpression of NADH-dependent enzymes can greatly increase the NAD^+/NADH ratio (Liu et al., 2012). Their gene expression can be modified to achieve metabolic flux by regulating the extracellular redox potential. Engineering processes such as energy input, redox reagents, and gas sparging can control the extracellular redox potential, indirectly influencing gene expression for bulk commodity production (Liu et al., 2017). Therefore, ORP regulation can influence hydrogen, pyruvate, propanediol, butanol, acetate, and ethanol production via fermentation (Liu et al., 2012; Liu et al., 2017).

2.2 MFC Sensor Overview

2.2.1 Background

In 1838, William Robert Grove, the father of fuel cells, pointed out that hydrogen could be used for power generation in a fuel cell. Fuel cells are power generation devices with no polluting gas emissions, higher efficiency, and lower sonic pollution (Rahimnejad et al., 2015). However, high temperature, cost, and corrosiveness impede fuel cell progress. Compared with conventional fuel cells, biological fuel cells (BFCs) continuously produce electricity while their cells are alive. Furthermore, their high efficiency, mild operating conditions, lower cost, and nontoxic by-products have garnered BFCs much attention (Rahimnejad et al., 2015; Khera & Chandra, 2012; Santoro et al., 2017). BFC devices convert chemical to electrical energy through electrons collected from electrochemical reactions in a biochemical pathway (Santoro et al., 2017). In 1911, Michael Cressé Potter used *Saccharomyces cerevisiae* and *Escherichia coli* with platinum electrodes to show that microorganisms can generate current in fuel cells. Therefore, MFCs were created, using whole microbial cells to react with biomass to produce bioelectricity. In 1931, Barnett Cohen discovered that MFC devices connected in series could produce more power. In 1987, Bennett made significant progress in MFCs, showing that mediators in anode compartments could help microorganisms sustainably produce electrons for weeks. This discovery greatly improved MFC service life. In 1991, Habermann and Pommer discovered that MFCs could produce electricity and treat sewage simultaneously, which is another commercial purpose besides power generation. Following more in-depth research, the electric power produced had increased 5–6-fold by 2009 (Beecroft, 2010; Santoro et al., 2017). However, MFC devices still have many problems that must be solved before they can be used in industry.

2.2.2 Working Principle of an MFC

An MFC is a bioelectrochemical reactor that uses anaerobic or microaerobic bacteria to oxidize organic or some inorganic compounds to produce electrons and waste in the anode chamber (Figure 2.2). The anode electrode receives the electrons, which are transferred to the cathode chamber through an external wire connected to the cathode electrode. A PEM aids proton transfer. Since the water in the cathode compartment is rich in oxygen, a reduction reaction occurs on the cathode electrode's surface, combining oxygen, protons, and electrons to form water (Beecroft, 2010; Rahimnejad et al., 2015).

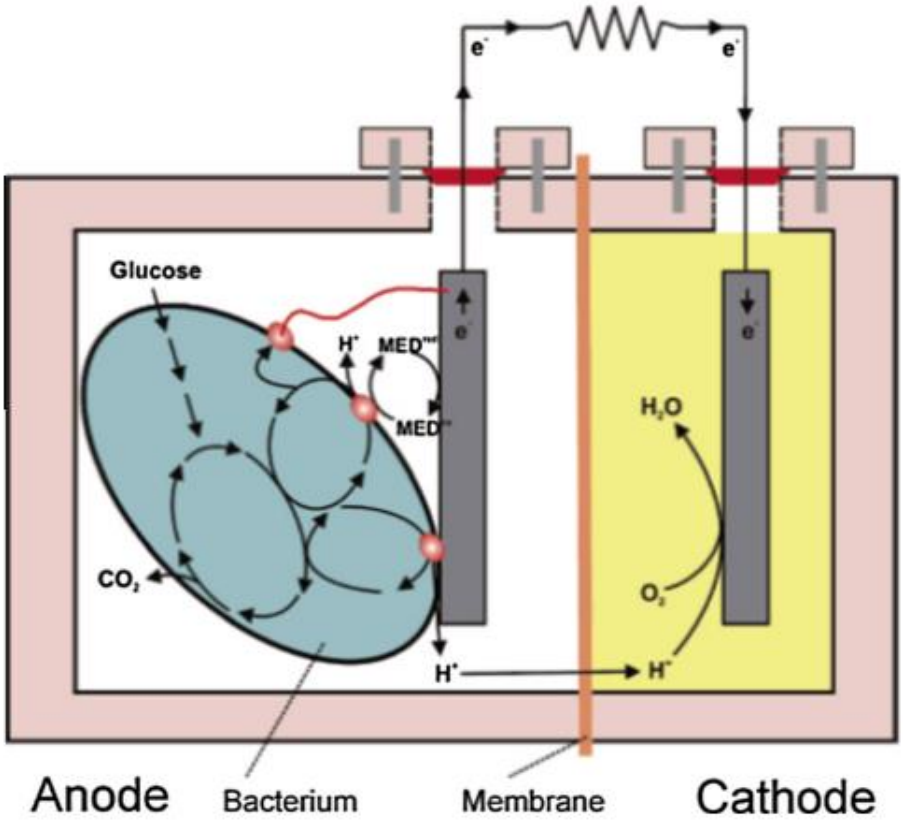

FIGURE 2.2 The general components and working principle of an MFC. The figure is reproduced from Logan et al., (2006). (Permission to reproduce is granted by American Chemical Society)

2.2.3 Applications

Most MFC research has focused on electricity generation. The MFC device can use various substrates to react with bacteria in an anaerobic anode compartment, producing relatively low

bioenergy (power) levels. Power output efficiency mainly depends on the oxidization rate, electrode materials, PEM material, and operation conditions. Bioelectricity from modern NFCs can charge small electrical devices, such as an LED lamp or a digital clock (Rahimnejad et al., 2015; Kumar et al., 2017).

During power generation, the MFC bioreactor can also treat wastewater simultaneously. For example, many inorganic and organic materials in wastewater can be used as substrates for microorganisms to produce electricity. Indeed, MFCs were shown to reduce the chemical oxygen demand (COD) of wastewater. MFCs can even achieve a 98% COD removal rate in wastewater treatment. Furthermore, unlike the conventional process, the MFCs can completely break down the substrates into carbon dioxide, water, electrons, and protons to produce less solid waste (Kumar et al., 2017; Karmakar et al., 2010).

Bioremediation is more environmentally friendly and cost-effective than traditional physical and chemical soil treatment because it mainly relies on the catalytic activity of indigenous microorganisms. However, the absence of electron acceptors in the soil will influence bioremediation performance (Li et al., 2017). MFCs can provide an inexhaustible anode in the soil to accept electrons and generate power. Electricity generated in an anaerobic environment can stimulate growth, activity, and oxidation-reduction reaction to accelerate biodegradation (Li et al., 2017).

Researchers have invested significant time and effort in increasing MFC output power generation. However, their results remain unsatisfactory. Therefore, the research focus shifted from power generation to other MFCs applications. Using MFC devices to monitor environmental conditions has received significant attention (El Mekawy et al., 2018). The MFC's anode compartment works as a bioreceptor to collect the electrons produced by microbial activity and convert them into a readable signal to reflect the real-time pollutant concentrations. The most significant difference between MFC power generation and MFC biosensors is their intended function. While MFC power generation devices mainly focus on power generation, MFC biosensors require a greater focus on sensitivity and stability (El Mekawy et al., 2018). MFC biosensors can detect biogas generation. In anaerobic environment conditions, MFCs can monitor current output fluctuation to estimate the biochemical oxygen demand (BOD), which can reflect the organic waste concentration. While

detecting heavy metals with an MFC biosensor only creates a low output voltage, sudden fluctuations can still be captured and used to analyze their concentrations (Zhou et al., 2017).

2.2.4 MFC Components

MFCs comprise an anode electrode (necessary), cathode electrode (necessary), anodic chamber (necessary), cathodic chamber (optional), PEM (necessary), electrode catalyst layer (optional), and external wire (necessary; Khera & Chandra, 2012; Du et al., 2007).

Anode compartment: The anode compartment comprises an anode electrode, substrates, and anaerobic microbes, which produce electrons, carbon dioxide, and protons by consuming the substrates. For example, glucose's oxidation reaction is shown in Eq. (2.6; Zhou et al., 2017; Dutta & Kundu, 2018; Rahimnejad et al., 2015). Glass, polycarbonate, and Plexiglas have been frequently used as anode chamber cover materials (Du et al., 2007).

$$C_2H_4O_2 + 2H_2O \rightarrow 2CO_2 + 8e^- + 8H^+ \quad (2.6)$$

Cathode compartment: The cathode chamber comprises a cathode electrode and oxidant. The protons generated in the anode compartment are transferred to the cathode compartment by the PEM. Electrons are transferred to the cathode chamber via an external wire. Air is pumped into the cathode chamber as the oxidant. The reduction reaction occurring in the cathode chamber is shown in Eq. (2.7; Dutta & Kundu, 2018; Rahimnejad et al., 2015). Glass, polycarbonate, and Plexiglas can be used as the outside cover materials (Du et al., 2007).

$$2O_2 + 8H^+ + 8e^- \rightarrow 4H_2O \quad (2.7)$$

Anode electrode: During the electroactive metabolic action, the electrons are collected by the anode electrode (Dutta & Kundu, 2018; ElMekawy et al., 2018). Anode materials should have high electronic conductivity, biocompatibility, chemical stability, specific surface area, and porosity. Therefore, materials such as graphite, graphite felt, carbon paper, carbon-cloth, Pt, Pt black, and reticulated vitreous carbon (RVC) can be used (Khera & Chandra, 2012; Du et al., 2007).

Cathode electrode: The cathode electrode accepts electrons from the anode chamber (Dutta & Kundu, 2018). The reduction reaction occurs on the cathode's surface for the terminal electron acceptors. The commonly used materials are graphite, graphite felt, carbon paper, carbon cloth, Pt, Pt black, and RVC (Du et al., 2007).

External wire: An external titanium wire is commonly used to transport electrons (Dutta & Kundu, 2018).

Catalyst: Pt, Pt black, MnO2, Fe3+, polyaniline, and platinum can optionally be used in the anode and cathode chambers to lower the activation energy and facilitate the reaction (Du et al., 2007; Dutta & Kundu, 2018; Rahimnejad et al., 2015).

PEMs: The PEM is a crucial MFC component separating the anode and cathode chambers, maintaining electro-neutrality between them, and facilitating proton transfer to sustain the current output (Tharali et al., 2016). Therefore, it should be made from materials with excellent stability, high ionic conductivity, low cost, low degradation, and high selectivity (Khera & Chandra, 2012), such as Nafion or Ultrex (Du et al., 2007).

2.2.5 Electron Transfer in MFCs

In MFC's anode chamber, microorganisms convert the substrates into electrons to maintain their growth. Microorganisms with an extracellular electron transfer ability could greatly influence bioreactor performance (Aiyer, 2020; Zhi et al., 2014). Since the solid electrode cannot penetrate bacterial cells to collect electrons, artificial electron shuttles were used to transfer electrons from inside cells to the anode electrode from an early stage (Schröder, 2007; Kumar et al., 2015). However, many artificial mediators, such as neutral red, methyl viologen, methylene blue, and thionin, were toxic and expensive, influencing MFC device scaling-up (Pinto, 2016). In recent decades, exoelectrogenic microbes were discovered, significantly improving MFC device performance (Zhi et al., 2014). Exoelectrogenic catalytic microbes exogenously transfer electrons to the electrode surface without artificial mediators (Kumar et al., 2016) because they can transport electrons from inside cells to the anode via redox-active cytochromes and conductive pili (direct electron transfer) or self-secreted flavins and pyocyanin mediators (self-mediated electron transfer; Kumar et al., 2016).

2.2.5.1 Direct electron transfer

Short-range direct electron transfer: The short-range electron transfer mechanism uses a redox-active protein to transport electrons from inside cells to an external electron acceptor (Figure 2.3A; Slate et al., 2019; Schröder, 2007). Multi-heme c-type cytochromes on the outer microbial membrane are responsible for electron diffusion (Slate et al., 2019; Pinto, 2016). Because electron transfer mainly relies on contact between cytochromes and the anode electrode's surface, power

generation will also rely on bacterial monolayer density (Schröder, 2007). The heme c-type cytochromes were first discovered in the *Geobacter sulfurreducens* genome (Kumar et al., 2015). Large numbers of cytochromes exposed on the outer cell surface improved the flexibility of the electron transfer network (Kumar et al., 2016). Cytochromes absence impeded power production, suggesting they act as a crucial electrochemical gate between the cells and the anode electrode's surface (Kumar et al., 2015).

Long-range electron transfer: Not all bacteria can attach to the electrode's surface to transfer electrons (Kumar et al., 2016). Therefore, exoelectrogenic bacteria also rely on conductive pili (nanowires) to transfer electrons to the solid electrode's surface (Figure 2.3B; Aiyer, 2020; Slate et al., 2019). The pili, or flagella, connect to the outer membrane cytochromes, enabling distant bacteria to transfer their electrons to the anode electrode (Aiyer, 2020). Nanowire formation allows a thicker biofilm to form on the anode electrode, greatly increasing MFC performance (Schröder, 2007). Long-range conductive pili were first found on *G. sulfurreducens* cells, increasing their power generation 10-fold (Kumar et al., 2015). *G. sulfurreducens*' type IV pili are conductive nanowires play an essential role in *G. sulfurreducens*' movement, adherence, and secretion system to establish connections between the bacterial cell and the electrode (Kumar et al., 2015; Slate et al., 2019).

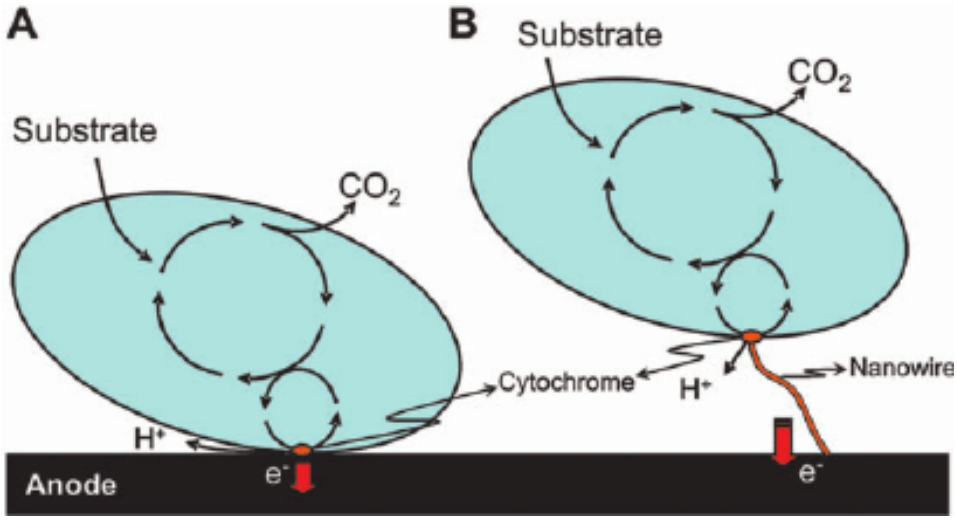

FIGURE 2.3 Illustration of (A) short-range and (B) long-range direct electron transfer. The figure is reproduced from Schröder (2007). (Permission to reproduce is granted by Royal Society of Chemistry)

2.2.5.2 Self-mediated electron transfer

Not all exoelectrogenic microbes can directly transport electrons to the anode electrode (Aiyer, 2020). Some strains secrete soluble electron shuttles to transport electrons from inside the cell to the electrode's surface (Beegle & Borole, 2018). Suitable redox mediators should have high membrane permeability, solubility, and electron transfer ability and be nondetrimental to microbial cells and nonbiodegradable (Bhunia & Dutta, 2018). Redox mediators can be primary or secondary metabolites (Schröder, 2007).

Secondary metabolites: Secondary metabolites can also be called endogenous redox or self-secreted mediators and include riboflavin, flavins, flavin mononucleotides, phenazines, phenothiazines, phenoxazines, pyocyanin, and quinones (Aiyer, 2020; Schröder, 2007; Bhunia & Dutta, 2018). Unlike direct electron transfer, the bacteria initially transport electrons to their surface via a metabolic pathway (Figure 2.4). Then, the electrons are transported by potential shuttles or cytochromes on the outer membrane to the electrode's surface (Slate et al., 2019; Schröder, 2007). Based on Gram-negative bacteria research, *Shewanella oneidensis* can be used to clearly explain this electron transfer type (Beegle & Borole, 2018). Besides acting as direct electron transport mediators, studies have discovered that outer membrane cytochromes such as MncA and MtrC are also associated with electron transfer (Beegle & Borole, 2018). MncA and

MtrC bind to redox mediators to help electrons transfer from the periplasm to the outer membrane (Kumar et al., 2016). Finally, soluble shuttles transport electrons to a suitable external acceptor.

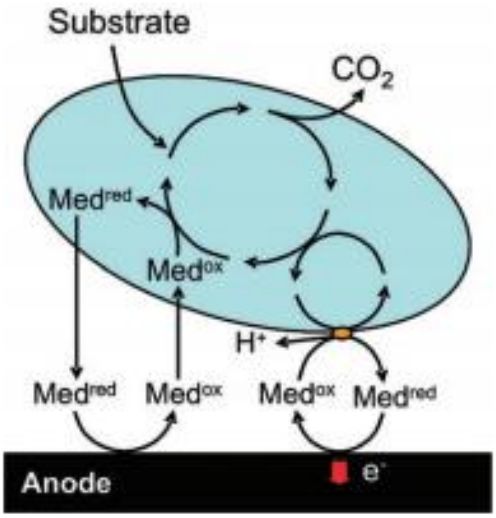

FIGURE 2.4 Illustration of electron transfer mediated through secondary metabolites. The figure is reproduced from Schröder (2007). (Permission to reproduce is granted by Royal Society of Chemistry)

Primary metabolites: Primary metabolites (indirect electron transfer mediators) can produce and transfer electrons from anaerobic respiration and fermentation (Beegle & Borole, 2018). When bacteria use an anaerobic respiration pathway (Figure 2.5A), electron acceptors with a reversible oxidation ability in the cell can act as electron shuttles (Schröder, 2007). The sulphate reduction reaction shown in Eq. (2.8) is a commonly studied anaerobic respiration electron transfer mechanism in *Desulfovibrio desulfuricans* (Schröder, 2007; Beegle & Borole, 2018).

$$(SO_4)^{2-} + 8H^+ + 8e^- \rightleftharpoons S^{2-} + 4H_2O \qquad (2.8)$$

As an external electron acceptor, sulphide oxidation plays a vital role in electron transfer in MFC devices, especially in wastewater treatment (Schröder, 2007). Unlike anaerobic respiration, the bacteria in the fermentation process transport electrons via bioproducts, such as hydrogen, acetate, ethanol, methanol, and formate (Figure 2.5B; Beegle & Borole, 2018). During fermentation, organic compounds are broken down into short-chain metabolites and electrons. Therefore, electrons will cluster with metabolites when touching the anode electrode for electron transfer (Schröder, 2007; Beegle & Borole, 2018).

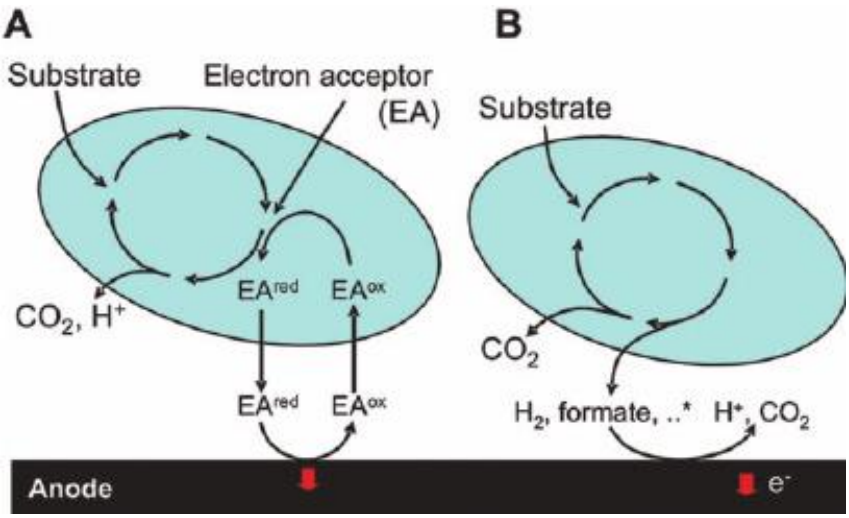

FIGURE 2.5 Illustration of electron transfer mediated through primary metabolites in the (A) anaerobic respiration and (B) fermentation pathways. The figure is reproduced from Schröder (2007). (Permission to reproduce is granted by Royal Society of Chemistry)

2.2.6 MFC Configuration

Fundamentally, reactor configuration plays an essential role in controlling costs and applications (Karmakar et al., 2010; Bhargavi et al., 2018). MFC devices have many uses, such as biosensors, metal recovery, and energy production, and some potential applications remain to be developed. Different MFC configurations are required to enable MFC devices to function under different conditions (Tamboli & Eswari, 2019). MFC designs can generally be classified as single-chamber or double-chamber (Jumma & Patil, 2016).

2.2.6.1 Double-chamber MFCs

Double-chamber MFCs are the earliest and most common design, comprising an anode and a cathode chamber separated by a PEM (Bhargavi et al., 2018; Tamboli & Eswari, 2019). Double-chamber MFCs are often run in a batch using a substrate and catholyte solution in the anode chamber to generate energy (Kumar et al., 2017). The cathode chamber used in waterworks acts as the electron terminal acceptor (Tamboli & Eswari, 2019; Flimban et al., 2018). Initially, the MFC device was built to study electrode materials and microbial activity and optimize parameters (Bhargavi et al., 2018). However, using the MFC to treat wastewater and produce electricity does not save energy because dry air must be pumped continuously into the cathode chamber (Bhargavi et al., 2018; Flimban et al., 2018). Furthermore, the relatively long distance between the two chambers decreased MFC performance (Flimban et al., 2018). However, double-chamber MFC

performance can easily be controlled by adjusting the pH, purging pure oxygen, increasing the flow rate, and adding an electron mediator (Flimban et al., 2018). H-shape, flat plate, up-flow, and miniature are common double-chamber MFC configurations.

H-shape: The H-shaped MFC type is suitable for examining parameters such as membranes, microbial communities, and electrode materials (Tamboli & Eswari, 2019; Jumma & Patil, 2016). In the H-shape double-chamber MFC, two bottles are connected by a tube with the membrane clamped in its middle (Singh et al., 2010). The total power produced by this system mainly depends on the surface area of the cathode relative to the anode and membrane. Because increasing the reactor size will decrease the total power output, up-scaling the H-shape MFC is complicated (Tamboli & Eswari, 2019; Singh et al., 2010).

Flat Plate: The cubic compact flat-plate MFC has mainly been used to generate power (Flimban et al., 2018; Min & Logan, 2004). In this system, a hot Nafion PEM is attached to the cathode and contacts the anode, with the two separate parts compacted with two nonconductive plates (Flimban et al., 2018; Min & Logan, 2004). The anode chamber is pumped continuously with wastewater or other organic biomass, and dry air is pumped continuously into a cathode chamber without any liquid catholyte (Flimban et al., 2018). The flat-plate continuous-flow MFC reactor system can generate 14 times more power than other MFC types (Flimban et al., 2018). Furthermore, because the flat-plate MFC can generate power from various organic substrates, it can be used to study and select the best combination of various microorganism-mediator-substrates to improve MFC performance (Tamboli & Eswari, 2019; Flimban et al., 2018).

Up-Flow: Up-flow MFCs have recently received greater attention (Kumar et al., 2017). Unlike conventional MFCs, the cathode and anode chambers of up-flow MFC are at the top and bottom. The PEM separating the two chambers has a 15° tilt relative to the ground to prevent gas bubble accumulation (Tamboli & Eswari, 2019). The wastewater or the organic substrates are pumped into the bottom of the anode chamber and flow out of the top of the cathode chamber (Kumar et al., 2017). Therefore, the up-flow MFC is suitable for wastewater and other carbon source treatment (Flimban et al., 2018). While one experiment using this MFC achieved 90% COD removal from domestic wastewater, total power generation and Columbia efficiency were not very high (Ismail & Jaeel, 2016). Fluid pumping and recirculation are required to make the device

operate normally. The up-flow MFC can only be used as an alternative wastewater treatment device due to its high energy consumption (Flimban et al., 2018; Ismail & Jaeel, 2016).

Miniature: The developed micro-sized double-chamber MFCs can be used as biosensors at remote or less-accessible sites because of their long-term power sources (Flimban et al., 2018; Wang et al., 2011). Furthermore, while micro-sized MFCs can immediately generate power without delays of hours or days, their total power output is very low (Wang et al., 2011).

2.2.6.2 Single-chamber MFCs

Following their development, single-chamber MFCs were designed to overcome some limitations of double-chamber MFCs (Tamboli & Eswari, 2019). Unlike the double-chamber design, the single-chamber design comprises an anode chamber and an air cathode chamber, so the aeration step for both MFC chambers can be eliminated to reduce energy consumption (Karmakar et al., 2010; Bhargavi et al., 2018; Flimban et al., 2018). Furthermore, because their interelectrode spacing is smaller, their internal resistance is also reduced (Kumar et al., 2017). A PEM or gas diffusion layer separates the two electrodes and stops oxygen from leaking into the anode chamber (Flimban et al., 2018). Like all other MFC devices, electricity is generated in the anode chamber. Oxygen from the air can be used for the cathode electrode (Jumma & Patil, 2016; Flimban et al., 2018). Single-chamber MFCs are easier to use and have higher oxygen reduction rates and lower internal resistances than double-chamber MFCs (Flimban et al., 2018). Single-chamber MFCs can better stimulate microbial activity. After monitoring the total petroleum hydrocarbon content in soil samples for 20 days, a single-chamber MFC achieved a 46.15% cleaning rate, higher than the 25.64% achieved by a double-chamber MFC. Single-chamber MFCs produce higher voltages than double-chamber MFCs. Moreover, the single-chamber MFC degraded more sediment pollutants and produced more power than the double-chamber MFC (Permana et al., 2020). Furthermore, single-chamber MFCs are better suited to monitoring remote sites and wastewater. During wastewater monitoring, rapid and accurate BOD data collection is essential for increasing treatment efficiency. Because the cathode electrode in a single-chamber MFC biosensor directly contacts air, its dynamic range will increase by 133%. Furthermore, a single-chamber MFC biosensor showed good reproducibility (0.53%), low response time, simple operation, and a steady-state current output (Di Lorenzo et al., 2009). Liquid leakage and oxygen diffusion are

common issues in single-chamber MFC applications (Flimban et al., 2018; Chatterjee et al., 2018; Saravanan & Karthikeyan, 2017).

2.2.7 MFC Performance

2.2.7.1 Idealized performance

Electricity is generally produced in MFC devices based on a thermodynamic reaction. This reaction can be explained using Gibbs free energy in Eq. (2.9), measuring the reaction's maximum work (Logan et al., 2006):

$$\Delta G_r = \Delta G_r^0 + RT \ln(\Pi), \tag{2.9}$$

where ΔG_r (in J mol^{-1}) is the change in Gibbs free energy for the specific conditions; ΔG_r^0 (in J) is the free energy under standard environmental conditions (298.15 K, 1 bar pressure, and 1 M concentration), calculated from the tabulated energies in organic compound water sources; R is the universal gas constant (8.31 J mol^{-1} K^{-1}), T (in K) is the absolute temperature; and Π (dimensionless) represents the reaction's products divided by its reactants (Logan et al., 2006). Furthermore, the Gibbs free energy change can reflect the maximum electric energy (Zhao & Xu, 2009). A more convenient approach to describe the MFC's maximum electric energy is to substitute Gibbs free energy in the cell electromotive force (E_{emf}; in V) equation, as shown in Eq. (2.10; Logan et al., 2006):

$$-\Delta G_r = E_{emf} Q, \tag{2.10}$$

where Q is the charge transferred in the reaction, which can also be substituted by $n \times F$, where n is the number of electrons exchanged in the reaction and F is Faraday's constant (9.65×10^4 C mol^{-1}). Therefore, the original Gibbs free energy equation in Eq. (2.9) can be rewritten in terms of E_{emf} (in V), as shown in Eq. (2.11; Logan et al., 2006):

$$E_{emf} = E_{emf}^0 - \frac{RT}{nF} \ln(\Pi). \tag{2.11}$$

2.2.7.2 Actual performance

Theoretically, numerous irreversible polarization losses can influence the maximum cell voltage (E_{emf}). In Eq. (2.12), the measured total power generation (E_{cell}) can be caused by the difference

between the theoretical measured cell voltage and electrode overpotentials and the system's ohmic loss (Logan et al., 2006; Mahadevan et al., 2014).

$$E_{\text{cell}} = E_{emf} - (\sum \eta_a + |\sum \eta_c| + IR_{\Omega}), \tag{2.12}$$

where $\sum \eta_a$ and $|\sum \eta_c|$ are overpotentials in the anode and cathode chamber, respectively, and R_{Ω} is the total cell internal ohmic resistance. The key overpotential loss types are activation polarization, ohmic losses, concentration polarization, and microbial metabolic activity losses (Du et al., 2007; Logan et al., 2006; Mahadevan et al., 2014).

Ohmic losses: Ohmic loss can be explained by resistance to the flow of electrons in the electrode and protons in the electrolyte, causing a voltage drop (Zhao & Xu, 2009). The PEM is a significant resistance that produces the transmembrane potential difference (Du et al., 2007). Ohmic losses can also be caused by the distance between electrodes (Ki et al., 2016). Therefore, using a highly-conductive anode material, checking all contacts thoroughly, increasing the solution's conductivity, and minimizing the electron's total travel distance can reduce ohmic losses (Logan et al., 2006; Mahadevan et al., 2014).

Activation losses: Electrode resistance and physicochemical surface reactant species adsorption will slow the electrochemical reaction on the electrode's surface (Zhao & Xu, 2009). Activation losses will also increase after proton accumulation, resulting in a lower cell potential (Oguz Koroglu et al., 2019). While activation losses can occur in both the anode and cathode chamber, the cathode always has a higher activation loss than the anode (Mahadevan et al., 2014). Increasing the anode's surface area, improving anode-microbe interactions, increasing the operating temperature, and adding a catalyst to the electrode can minimize this issue (Mahadevan et al., 2014).

Microbial metabolic losses: While microorganisms derive energy from their catabolism of organic compounds, a voltage loss will happen simultaneously (Mahadevan et al., 2014). Liberating the electrons from substrates is crucial for sustainable electricity generation in MFCs (Aelterman et al., 2008). In the anode chamber, the anode potential is produced by the oxidation reaction of microorganisms and influences electron liberation. Higher total anode potentials increase the microorganism's growth rate and biocatalyst density, resulting in a higher current generation (Aelterman et al., 2008). However, the anode potential should be as low relative to the cathode

chamber as possible to achieve maximum power (Logan et al., 2006; Aelterman et al., 2008). Microbe types, anode-microbe interactions, excessive biomass, fuel degradation rate, and microbial activity can also cause microbial metabolic losses (Mahadevan et al., 2014).

Concentration losses: To maintain the power density output, the substrates and oxidants must be continuously supplied (Du et al., 2007). Substrates are transformed into protons and by-products in the anode chamber. However, according to Nernst, the voltage output will decrease when the total product concentration exceeds the reactant concentration (Yang et al., 2021). The same concept can be applied to air supplementation in the cathode chamber. Therefore, limited substrate supplementation to biofilms and insufficient oxygen supply at the cathode electrode's surface will significantly reduce the power output (Mahadevan et al., 2014; Yang et al., 2021). Increasing the reactant concentration, decreasing the protons concentration, modifying the electrode, and creating a new cathode compartment design can minimize concentration losses (Oguz Koroglu et al., 2019; Yang et al., 2021).

2.3 Knowledge Gap and Objectives

In Appendix A, using only an ORP or MFC sensor to detect the microbial activity can reflect general microbial growth status. However, a novel ORP and MFC-based sensor could be more sensitive to reflect detailed microbial growth characteristics. Shen's dissertation (Shen, 2022) designed an H-shape double-chamber MFC sensor combined with an ORP sensor to relate information about the MFC voltage output, redox potential, and modified Nernst equation. Incorporating these data could realize some in-depth microbial growth characteristics. The utimate goal for our lab is to apply this MFC and ORP based sensor for in situ bioremediation application. However, the H-shape sensor was too large to be applied for in situ soil bioremediation for the pervious work. Therefore, for this project a novel miniature plugged-type MFC and ORP-based biosensor is designed and reported here. The fabricated portable sensor was placed in a lysogeny broth (LB) medium and cultured with *Bacillus subtilis* to test its workability at first.

3 MATERIALS AND METHODS

3.1 *B. subtilis*

The sensor's workability was tested using *B. subtilis*, a gram-negative bacteria that is non-pathogenic, easily found in soil, and commonly used to produce commercial products (Piggot, 2009). *B. subtilis* can grow under anaerobic or micro-aerobic environmental conditions due to its nitrate electron acceptor (Hartig & Jahn, 2012; Piggot, 2009). The pH and ambient temperature always have an enormous effect on microorganism growth. However, *B. subtilis* can grow at pHs between 4.9 and 9.00 and temperatures between 15°C and 54°C (Gauvry et al., 2021). Furthermore, when *B. subtilis* is placed in proper growth conditions, it rapidly germinates and returns to vegetative growth (Piggot, 2009). Besides its great ability to adapt to the environment, *B. subtilis* can directly transfer electrons to the anode electrode through flavin without relying on artificial mediators (Chen et al., 2019; Ismail & Jaeel, 2013). Initially, 150 mL of LB medium (10 g/L peptone, 10 g/L sodium chloride, and 5 g/L yeast extract) was prepared and autoclaved for 20 minutes. It was used to culture *B. subtilis* spores in a shaker overnight at 120 rpm and 37°C. A single colony was isolated by taking one drop of the sample and streaking it on agar plates, which were incubated overnight at 37°C. Then, an single colony was picked from the petri dish, transferred to 150 mL of fresh LB medium, and cultured overnight at 37°C until it reached an OD of 3.5 at 600nm. An optical microscope was used to confirm if the *B. subtilis* cells has rod shape (Figure 3.1).

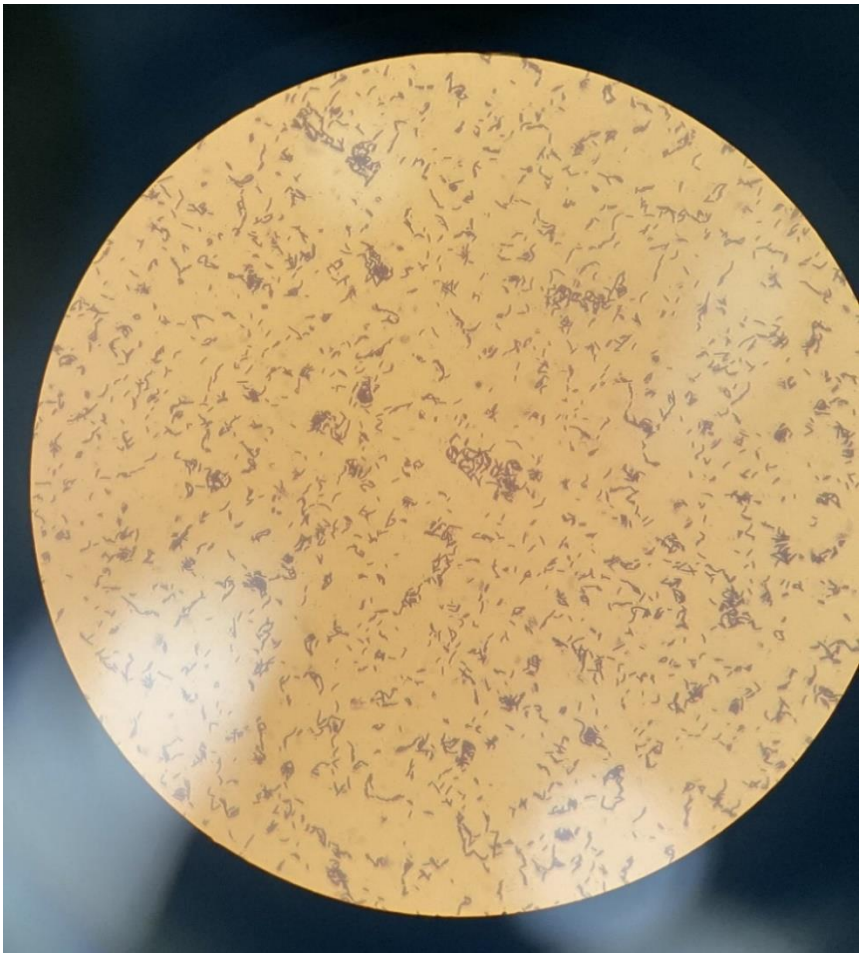

FIGURE 3.1 The morphological characteristics of B. subtilis in LB medium.

Each colony on the agar plate should be circular with a rough surface; opaque, fuzzy white, or slightly yellow colour; and jagged edges (Figure 3.2; Lu et a., 2018). The surplus inoculum was mixed with 60% glycerol for long-term strain preservation. Each microtube contained 0.5 mL of glycerol mixed with 0.5 mL of inoculum and stored in a −80°C freezer.

FIGURE 3.2 The characteristics of B. subtilis colonies on an agar plate.

3.2 Preliminary Sensor Configuration and Operation

3.2.1 Preliminary sensor

In the early-stage design (Figure 3.3), the anode electrode (carbon felt), PEM (Nafion 117), and cathode electrode (carbon cloth) were glued together with epoxy resin into a polypropylene (PP) bottle. However, epoxy did not prevent the solution from leaking into the bottle. Therefore, in the second version (Figure 3.4), two bottles were screwed together with the carbon cloth and Nafion 117 inside. A small opening was used for proton transfer. As the anode electrode, a large square carbon felt was directly tied to the bottle's outer surface. While the previous problems were solved, the computer did not receive a stable digital signal during the experiment, potentially due to the PEM's small active surface area. Therefore, the preliminary sensor's final version was designed based on the experiences of the two failed designs. Two PP bottles made the reactor chamber (Figure 3.5), with the carbon felt, PEM, and O-ring compressed in between. The open space at outer surface of PP bottle was large enough to enable the anode electrode to be directly inserted.

Because the ORP sensor is a very mature commercial product, it was not necessary to design a new ORP sensor for this project.

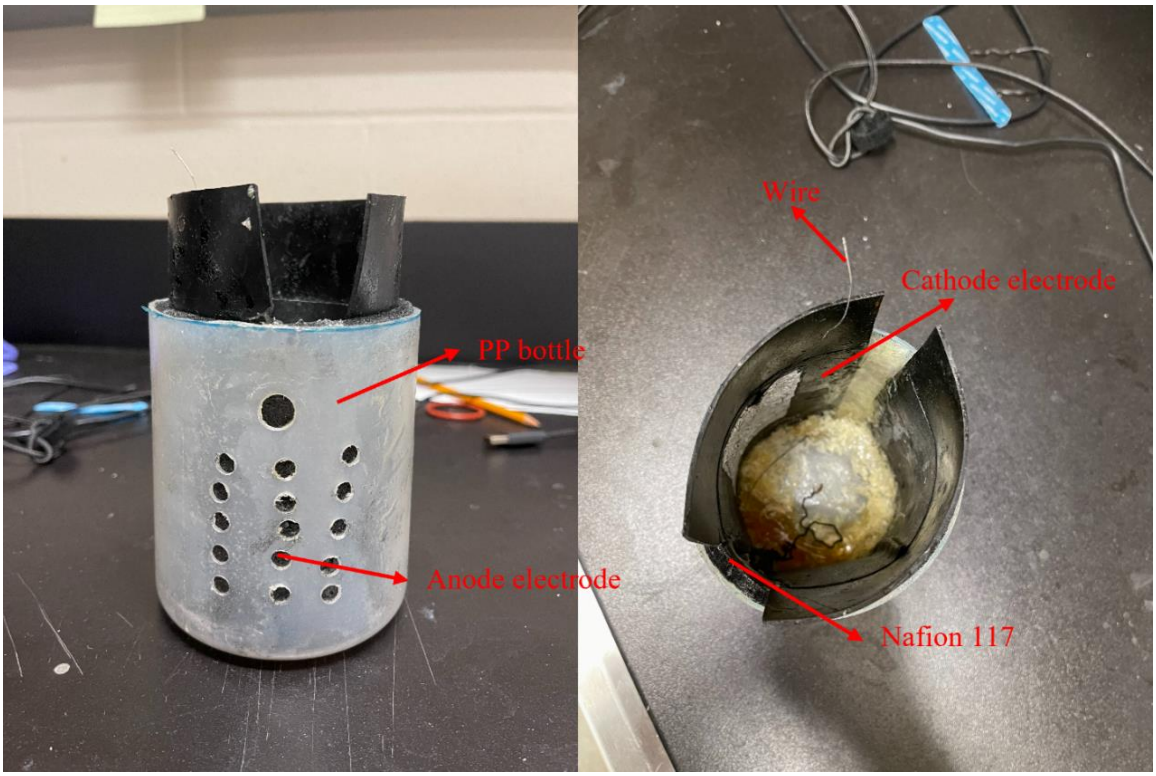

FIGURE 3.3 The first version of the preliminary MFC sensor.

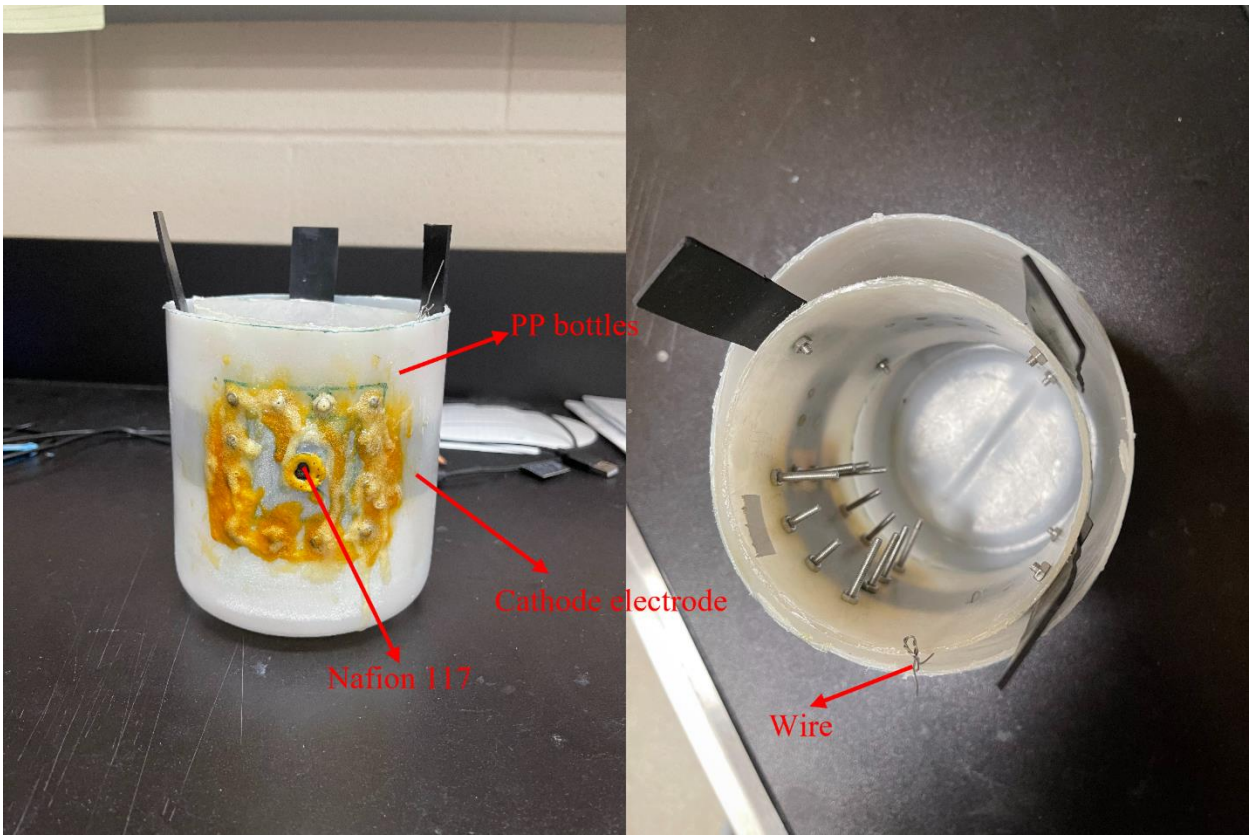

FIGURE 3.4 The second version of the preliminary MFC sensor.

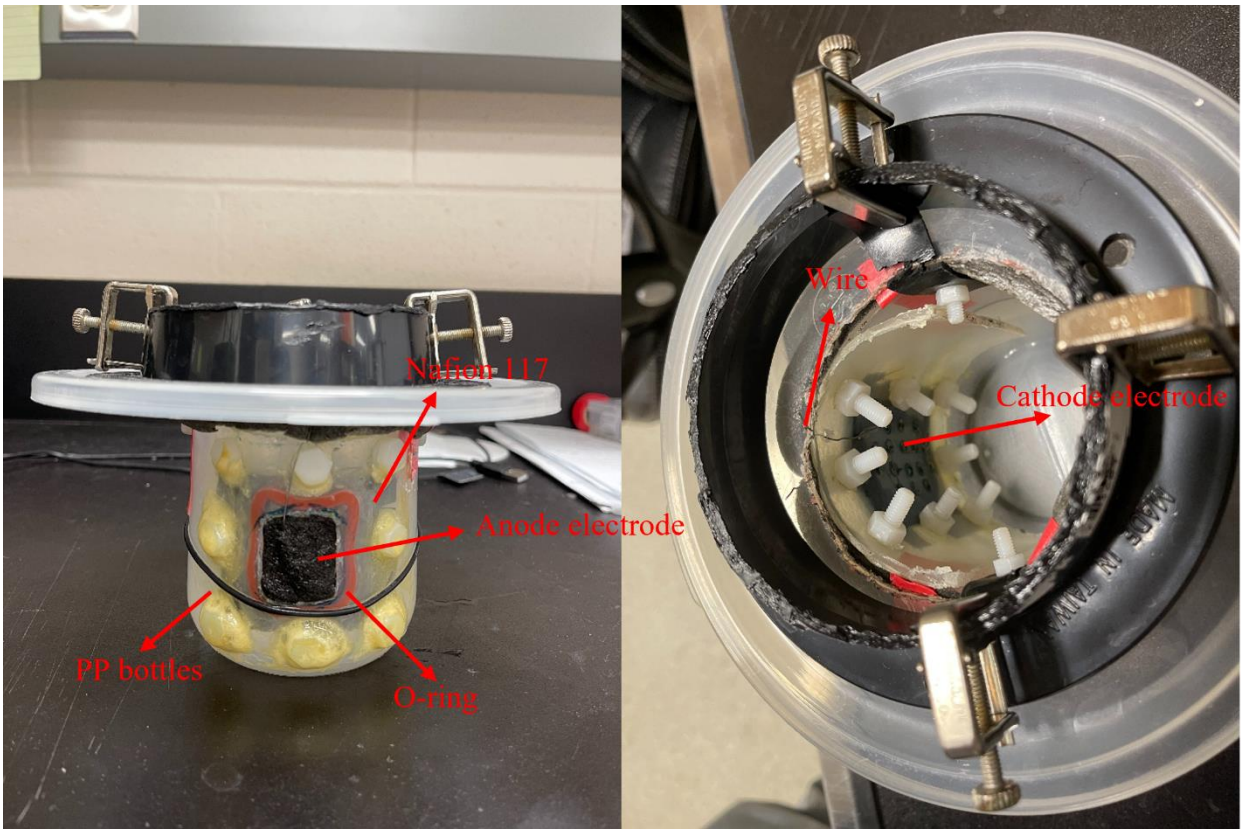

FIGURE 3.5 The final version of the preliminary MFC sensor.

3.2.2 Materials Description

Carbon-based materials such as carbon felt, graphite rod, and carbon mesh can be used for the anode electrode because they have suitable properties such as biocompatibility, long durability, good conductivity, low cost, and variable morphologies (Kalathil et al., 2018). The material used for the anode electrode can generally be used for the cathode but with an extra catalyst layer (Mustakeem, 2015). Because the catalyst layer helps the electrode accept protons, without it, the whole reaction happens very slowly (Khilari & Pradhan, 2018). Xue et al. (2011) reported that a 1 mg/cm^2 60% Pt/C cathode catalyst layer could efficiently increase MFC performance. Therefore, this bioreactor used a 0.5 mg/cm^2 60 Pt/C carbon cloth (Fuel Cell Store CO., USA). The PEM is crucial for the MFC device, separating its anode and cathode chambers, preventing air or solution leakage, and helping proton transfer. While various membrane types could be used for this novel MFC sensor, an MFC with Nafion 117 provided the greatest power generation (Ghasemi, 2015). Finally, titanium wire has a higher electrochemistry performance than steel wire for long-term

electric collection because titanium does not influence mass transfer and microbial growth (Jung et al., 2018).

3.2.3 Dimensions

Because the prices of Nafion 117 and Pt-covered carbon cloth are extremely high, the accessible area's appropriate size should be determined based on calculations and experiment reports. According to Appendix B, the total proton transfer through Nafion 117 per second is:

$$8.9\times10^{-4}\ (\text{mol/g}) \times 1.98\ (\text{g/cm}^3) = 1.76\times10^{-3}\ (\text{mol/cm}^3) \quad (3.1)$$

The total protons transferred per second through each square centimetre of Nafion 117 is:

$$1.76\times10^{-3}\ (\text{mol/cm}^3) \times 0.0187\ (\text{cm}) = 3.3\times10^{-5}\ (\text{mol/cm}^2) \quad (3.2)$$

Because the initial pH of 1 L of inoculum was 7.5, the initial ion concentration in the solution is:

$$\text{ion concentration } [H^+] = 10^{-7.5} = 3.16\times10^{-8}\ \text{M} \quad (3.3)$$

Based on the previous calculation, the minimal PEM area is:

$$3.16\times10^{-8}\ \text{M} \times 1\ \text{L} = 3.16\times10^{-8}\ (\text{mol}) \quad (3.4)$$

$$3.16\times10^{-8}\ (\text{mol}) \div 3.3\times10^{-5}\ (\text{mol/cm}^2) = 9.58\times10^{-4}\ (\text{cm}^2) \quad (3.5)$$

Therefore, the smallest active PEM size that could be used was 9.58×10^{-2} mm^2. However, many protons are released by the oxidation reaction during microbial growth. Therefore, the PEM actual size should enable those protons to pass rapidly. Suppose many protons are produced and cannot promptly transfer to the air cathodic chamber. Then, the remaining protons in the anode chamber will make the solution acidic and interrupt the microorganism's growth. The preliminary MFC sensor used a 50 mm high × 50 mm wide PEM. The O-ring size was chosen based on the membrane size, with a 43 mm outer diameter and 36 mm inner diameter. Therefore, the active PEM area of this preliminary sensor was 327 mm^2. Based on a large body of past MFC device construction research, the anode and cathode electrodes should always have a larger surface area than the PEM (Oh et al., 2004; Chaudhuri & Lovely, 2003; Bond & Lovely, 2003; Boas et al., 2019). Therefore, in the preliminary MFC sensor, the carbon felt anode electrode was 20 mm high × 25 mm wide ×

2 mm thick, and the carbon cloth cathode electrode was 50 mm high × 50 mm wide × 0.36 mm thick.

3.2.4 Material Pretreatment

Material pretreatment is especially important for achieving high sensor performance. Pretreatment of the anode electrode's surface can increase microorganism adhesion for better biofilm formation (Mustakeem, 2015; Kalathil et al., 2018). The carbon felt (Shi Ding Xian Inc., Ltd., China) was placed in an acetone solution to remove organic residues. After the electrode was completely dry, it was placed in a nitric acid (5% v/v) solution for 10 hours at 80°C. Finally, the treated electrode was rinsed with distilled water until a neutral pH was achieved and dried again (Hidalgo et al., 2016). This treatment's benefits are increased positive surface charges, reduced anode resistance, and enhanced surface roughness (Mustakeem, 2015; Kalathil et al., 2018). PEM (Nafion 117, DuPont, USA) pretreatment is necessary to remove any impurities and achieve higher performance (Rahimnejad et al., 2012; Ghasemi et al., 2013). First, the PEM was placed in 3% hydrogen peroxide for 1 hour. Then, after washing with deionized water, it was placed in 0.5 M sulfuric acid for another 1 hour. Finally, it was soaked in deionized water for 1 hour to wash off the attached acid. The entire process was performed at ~80°C. PEMs should be stored in deionized water until needed (Rahimnejad et al., 2012; Ghasemi et al., 2013; Kuwertz et al., 2016).

3.2.5 Experiment Setup

The experimental setup for the preliminary sensor is shown in Figure 3.6. To evaluate the preliminary sensor's performance, around 15 mL of *B. subtilis* culture solution from the flask was transferred into a bucket (2 L; Fu Xin Technology Co., Ltd., Guangdong, China) with 1 L of LB medium and cultured until it reached an initial OD of 0.1 at 600 nm. Around 4 mL of 1M sodium hydroxide was injected to adjust the initial pH to 7.5. The MFC sensor was fixed to the lid and inserted into the medium. Small holes were drilled to insert a pH meter, ORP sensor, and plastic tube. One head of the gas flowmeter (Sheng Jing Qi Wang Luo Ke Ji Co., Ltd., Guangdong, China) was connected to an air pump with a 0.5 vvm air sparging rate. The other head was connected to the plastic tube on the lid. Additionally, a magnetic stir bar was placed in the medium, and the bucket was placed on a stir plate set at 100 rpm to facilitate microbial growth and medium aeration (Jones et al., 2007). The whole experiment was performed at room temperature (23°C). Before setup, all components were wiped with 75% ethanol and exposed to ultraviolet (UV) light for 1 hour. Because *B. subtilis* can secrete exopolysaccharides and proteins to form the extracellular

polymeric substance biofilm, the anode electrode was soaked in 2M sodium hydroxide at the end of each experiment (Vlamakis et al., 2013; Antoniou & Frank, 2005; Rushdy & Othman, 2011). Other components were wiped with ethanol and exposed to UV light before subsequent use.

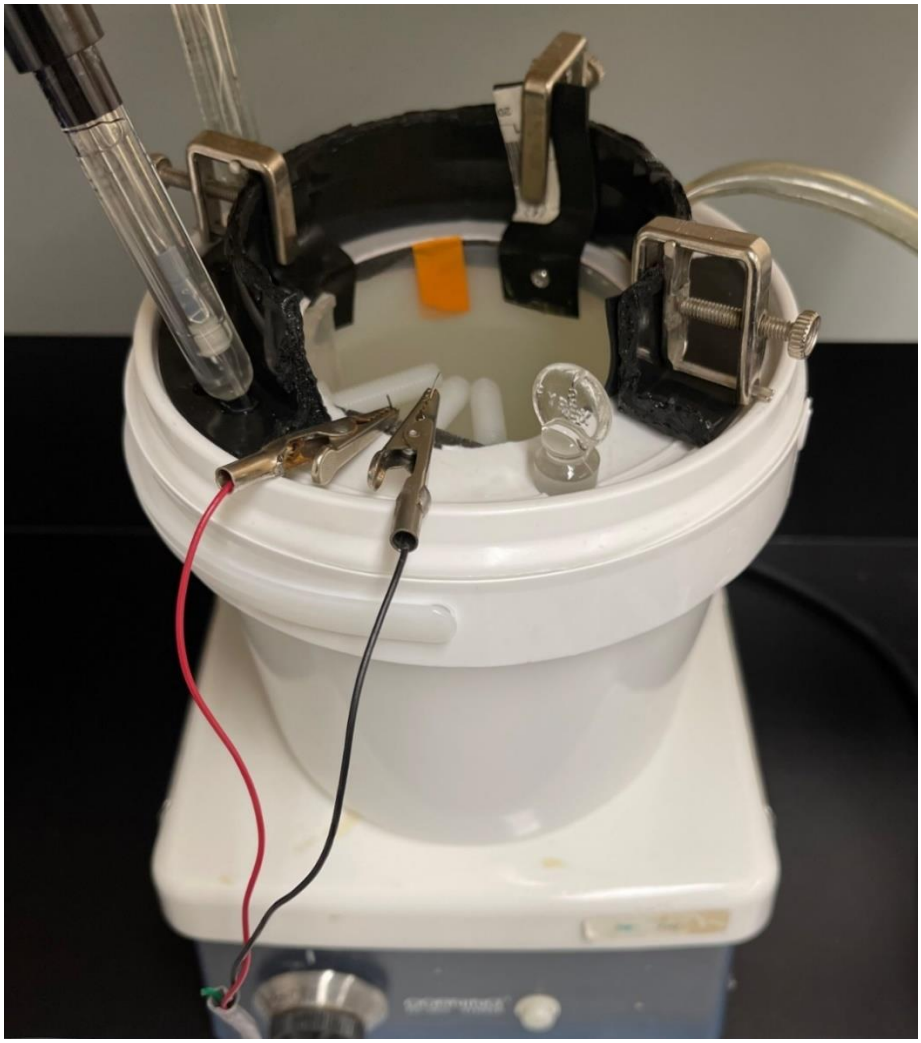

FIGURE 3.6 Experimental setup of the preliminary MFC and ORP-based sensor.

3.3 3D-Printed Sensor Configuration and Operation

3.3.1 3D-printed Sensor

After successfully using the preliminary MFC sensor in several experiments to acquire detailed microbial growth characteristics, a smaller MFC sensor was designed.

A 3D printer (FlashForge Inc, Zhejiang, Hangzhou, China) with a polylactic acid (PLA) filament (Polymaker LLC, Bluffton, SC, USA) was used to achieve a smaller size and ease of assembly.

The drawing software (SketchUp, Trimble Inc, Boulder, CO, USA) was initially used to design the appearance and some internal details. The material object from the 3D printer is shown in Figure 3.7. Initially, cylindrical-shaped PP bottles were chosen for the preliminary MFC sensor. Two PP bottles tightly compressed by screws formed the sensor's outer case. Due to the physical strength of the PLA filament used in the 3D-printed sensor, the shape was changed from cylindrical to cuboidal.

The novel miniature sensor was fabricated with the same design concept as the previous preliminary sensor. The components of the novel 3D-printed MFC reactor are shown in Figure 3.8. The novel 3D-printed MFC sensor comprised a three-sided cuboid (TSC) outer shell and a hollow cuboid (HC) inner shell. A circular recess was made on the TSC's inner side, which held a large O-ring (Figure 3.9). The front of the TSC included a circular hatch the same size as the large O-ring's inner diameter. The carbon felt was directly inserted into that opening. There was a cylindrical opening at the bottom of the TSC, and a circular groove was made around it to hold a small O-ring. When the ORP sensor was inserted through this O-ring, it formed a tight seal, preventing the solution from leaking into the cathode chamber. Some small round holes were drilled in the front of the HC to let the cathode electrode contact air (Figure 3.10). Some square clamps were designed to secure the TSC and HC chambers.

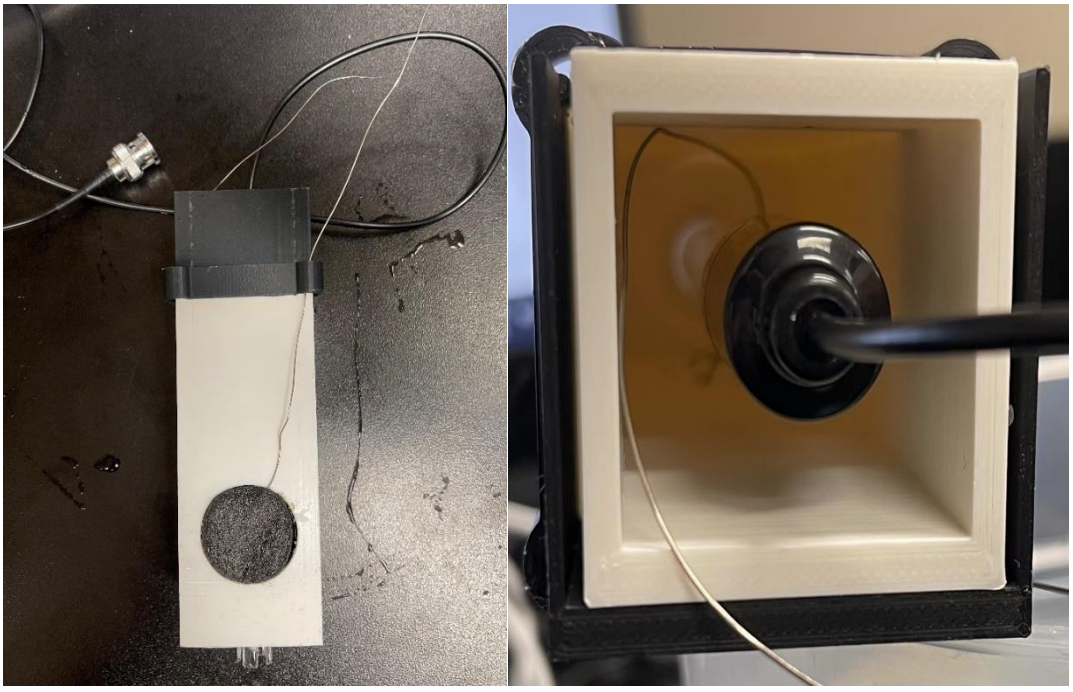

FIGURE 3.7 The configuration of the 3D-printed MFC and ORP-based sensor.

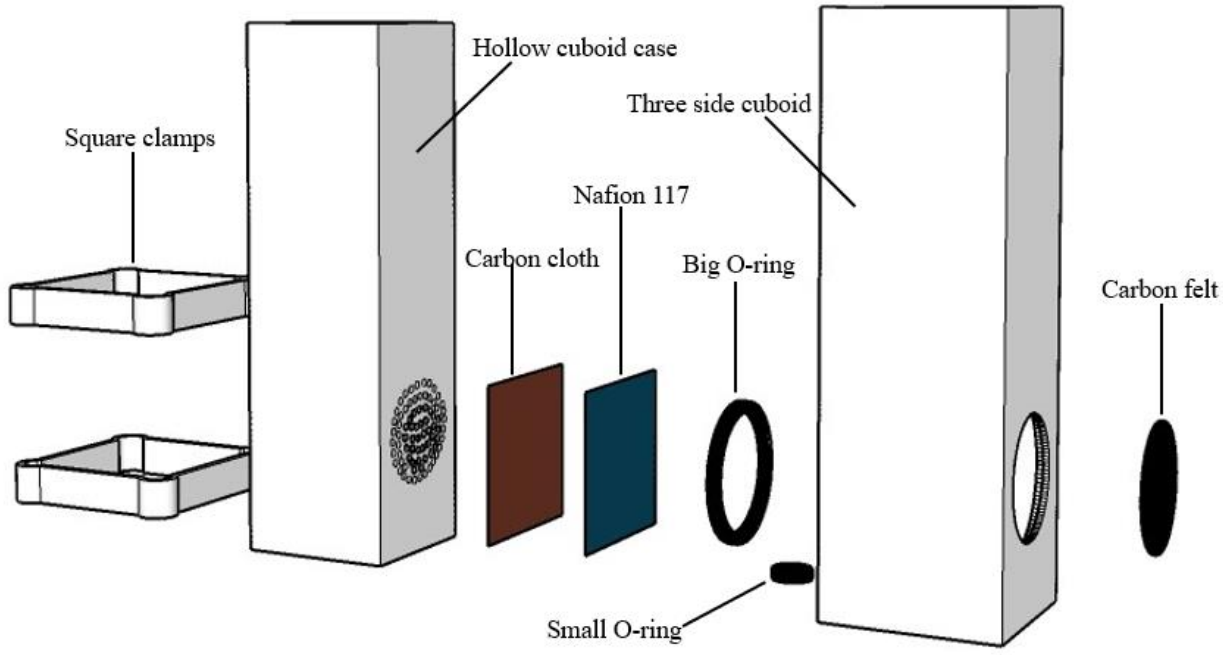

FIGURE 3.8 The components of the 3D-printed MFC sensor.

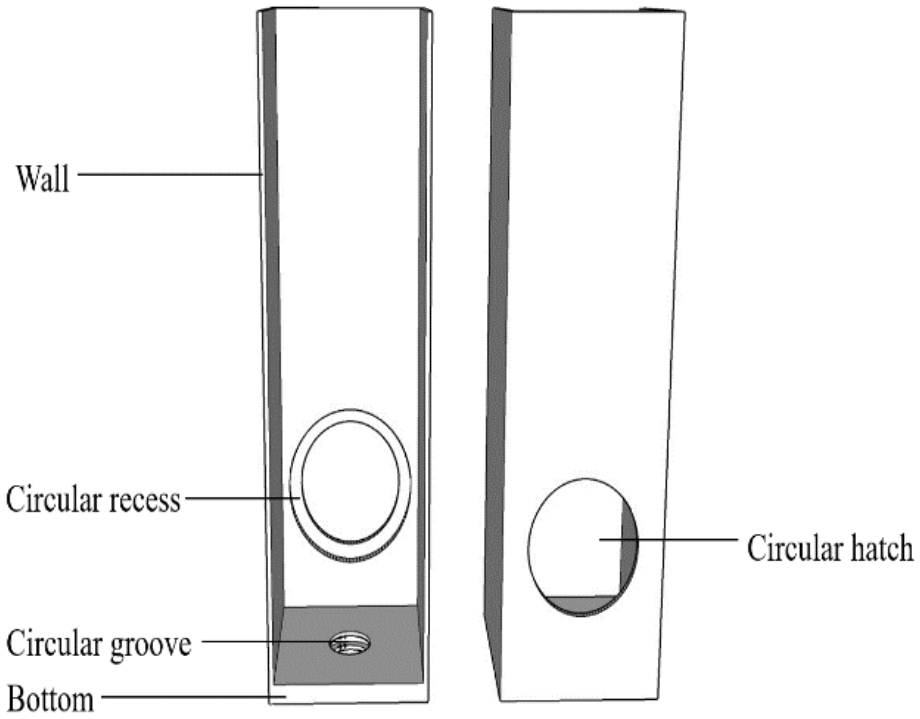

FIGURE 3.9 The TSC case design.

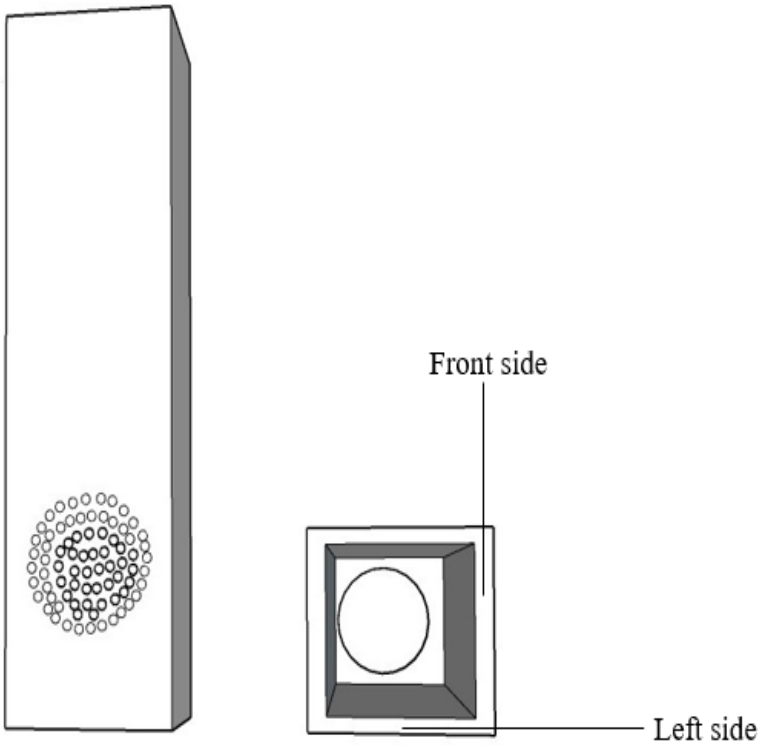

FIGURE 3.10 The HC case design.

3.3.2 Dimensions

The ORP sensor (ASR2803-3-1M-BNC) for lab use obtained from the Phidgets Company (Edmonton, AB, Canada) was 12 mm in diameter and 140 mm in length. Therefore, the HC should have sufficient inner space to house the ORP sensor with enough room for air exchange. The HC was 40 mm long × 40 mm wide × 138 mm high. The wall should be thick enough to ensure the cuboid's rigidity. The front and back walls were 4 mm thick, and the left and right walls were 3 mm thick.

The TSC was 44 mm long × 44 mm wide × 142.3 mm high. Its left and right walls were 1.3 mm thick. The big O-ring had a 3.5 mm cross-section, and the recess depth was 2.5 mm. The front wall was 4 mm thick to retain sufficient space for the O-ring recess. The large O-ring used had a 30 mm inner diameter and a 37 mm outer diameter. Therefore, the circular recess was 37 mm in diameter, and the circular hatch was 30 mm in diameter. The bottom was 4.3 mm thick. Based on the ORP sensor's size, the cylindrical hollow on the bottom of the TSC was 12 mm in diameter and 4.3 mm in height. A 10 mm inner diameter small O-ring was used to prevent leakage. Because the small O-ring had a 2.5 mm cross-section, the circular groove was 1.5 mm deep.

According to the previous calculation (3.5), the 30 mm diameter PEM used in the 3D-printed sensor provided an active area of 706.5 mm^2, much greater than its minimum value (9.58×10^{-2} mm^2). A 40 mm long × 40 mm wide Nafion 117 was used based on the O-ring's size. According to the preliminary design, the anode and cathode areas must be larger than the PEM active area. For the 3D-printed MFC sensor, the anode electrode was 30 mm in diameter and 2 mm in depth with total area 895 mm^2, and the cathode electrode was 40 mm in length and 40 mm in width with total area 1600 mm^2.

3.3.3 Experiment Setup

The 3D sensor's experiment setup is shown in Figure 3.11. The same parameters used with the preliminary MFC sensor were initially used in this experiment to test the new model's workability and accuracy. Because the smaller MFC sensor will influence microbial growth and accepted signals, some minor adjustments were made.

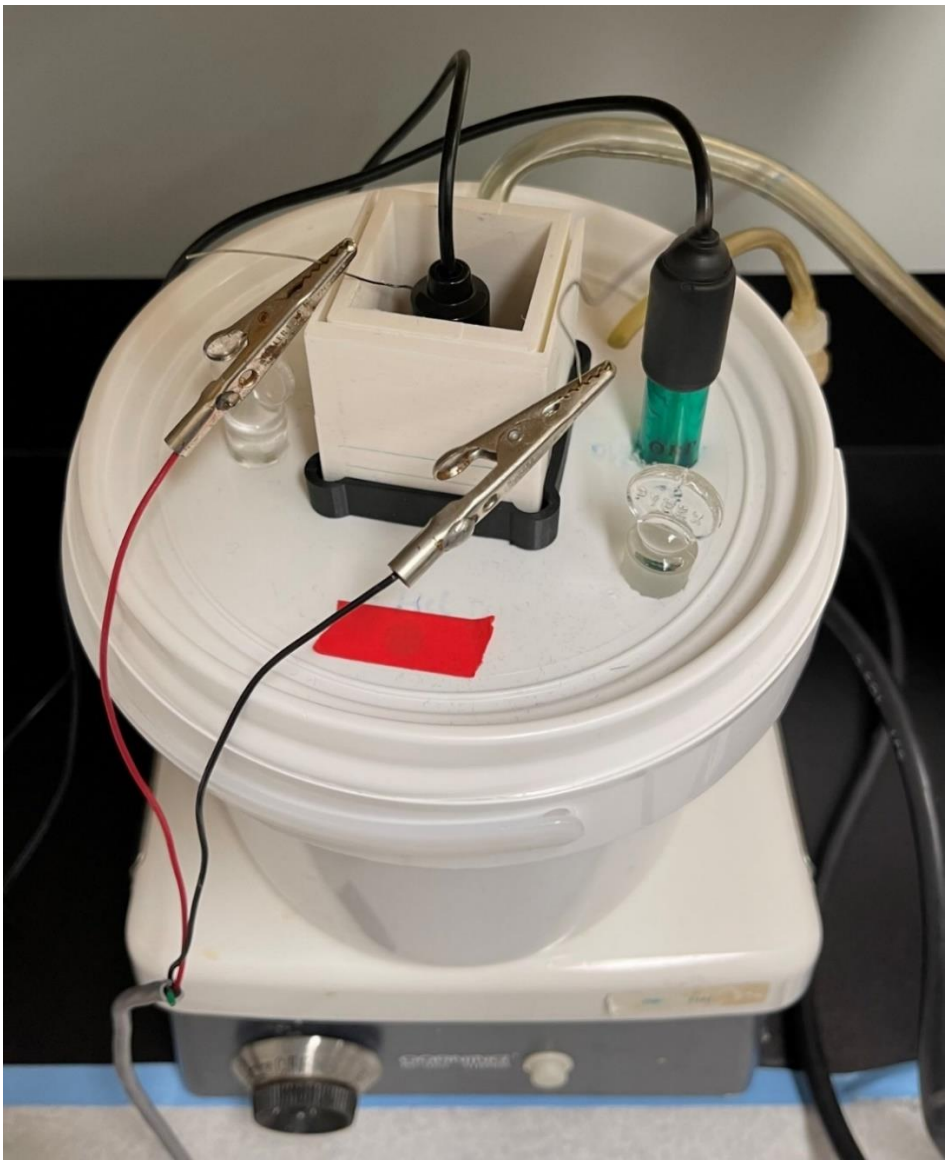

FIGURE 3.11 Experimental setup for the 3D-printed MFC and ORP-based sensor.

3.4 Voltage Output, Redox Potential, and Optical Density Analyses

Data collection was identical for the preliminary and 3D-printed integrated sensors. The voltage measured by the MFC sensor was transferred to the computer via a Phidgets VINT hub (Phidgets Co., Ltd., Edmonton, AB, Canada), which converted the voltage into a digital signal. Then, the computer-based data acquisition system (National Instruments, LabVIEW, version 19.0f2) recorded the digital data at 300-s intervals. The redox potential value was measured by the ORP sensor and a pH/temperature/mv/ISE multi-meter (VWR Scientific, PA, USA). A camera was installed before the meter to record the real-time redox potential value every 30 minutes. The

potential parameter value was calculated from the voltage and redox potential values using the modified Nernst equation e.g., Eq. (2.7) (Shen, 2022). A medium sample must be simultaneously tested to confirm that the potential parameter represents the microbial growth rate. After placing the sample into a benchtop spectrophotometer (UVmini-1240, Shimadzu Co., Ltd., Kyoto, Japan), its biomass concentration was determined based on the OD value at 600 nm.

$$Q = e^{-\frac{ORP}{Voltage}} \tag{2.7}$$

4 RESULTS AND DISCUSSION

First, several experiments were conducted to determine the optimal air sparging rate by keeping the agitation rate at 100 rpm. An air sparging rate of 0.50 L/min (i.e., 0.5 vvm) with an agitation rate of 100 rpm was the optimal *B. subtilis* growth condition for which both the preliminary and 3D-printed sensors identified the growth stage. While the growth conditions were the same for each experiment, the *B. subtilis* growth status was not. Appendix C shows three consecutive experiments testing the workability of the reported preliminary and 3D-printed sensors under the same experimental conditions and optimal air sparging rate. A representative high-resolution graph was selected for the preliminary (Figure 4.1) and 3D-printed (Figure 4.2) sensor.

4.1 Monitoring microbial growth with the preliminary sensor

From 0 to 5 hours, the potential parameter showed an increasing trend (Figure 4.1). Based on the derivative OD measurement, microbial growth after 4 hours was 0.06/hr, and after 5 hours was still 0.060/hr, indicating a slowly increasing total population in the medium. Therefore, microbial growth was in the lag phase.

After 6 hours, the derivative OD value rapidly increased (0.10/hr), and the potential parameter also dramatically increased, indicating that *B. subtilis* had entered the exponential phase.

After 6.5 hours, the potential parameter reached its first peak of 4.19. After 7 hours, the derivative OD value reached its highest value of 0.13/hr. While a bacterial population in the exponential phase starts to experience binary growth, metabolic activity in the early exponential phase still remains lower speed (Sood et al., 2011; Alberghina et al., 1975). After bacteria reaches the mid-exponential phase, the total population begins duplication growth (Alberghina et al., 1975; Keren

et al., 2004). Therefore, the first peak represents *B. subtilis* approaching its fast growth rate. Because of infrequent sampling, there will be a small difference between derivative OD and potential parameter peaks. While the portable sensor and spectrophotometer can detect the fast growth period, the spectrophotometer sample requires collection and pretreatment.

After 18 hours, the potential parameter's second peak of 3.0 appeared. After 19 hours, the derivative OD value did not change appreciably with time, indicating that the growth phase had begun to change from exponential to stationary growth. In the stationary phase, the newly evolved strain will kill or inhibit the growth of the parent strains, causing the total population to cease growing. Because bacteria still reproduce under starvation conditions, the stable population will persist for a while (Jaishankar & Srivastava, 2017). Therefore, the second peak acquired by the preliminary sensor is an indicator of the stationary phase's turning point. Because of the sampling time, there was a small difference between the derivative OD and potential parameter values.

After 18 hours, a gradual decrease in the potential parameter was accompanied by a stable derivative OD value until the end of the experiment.

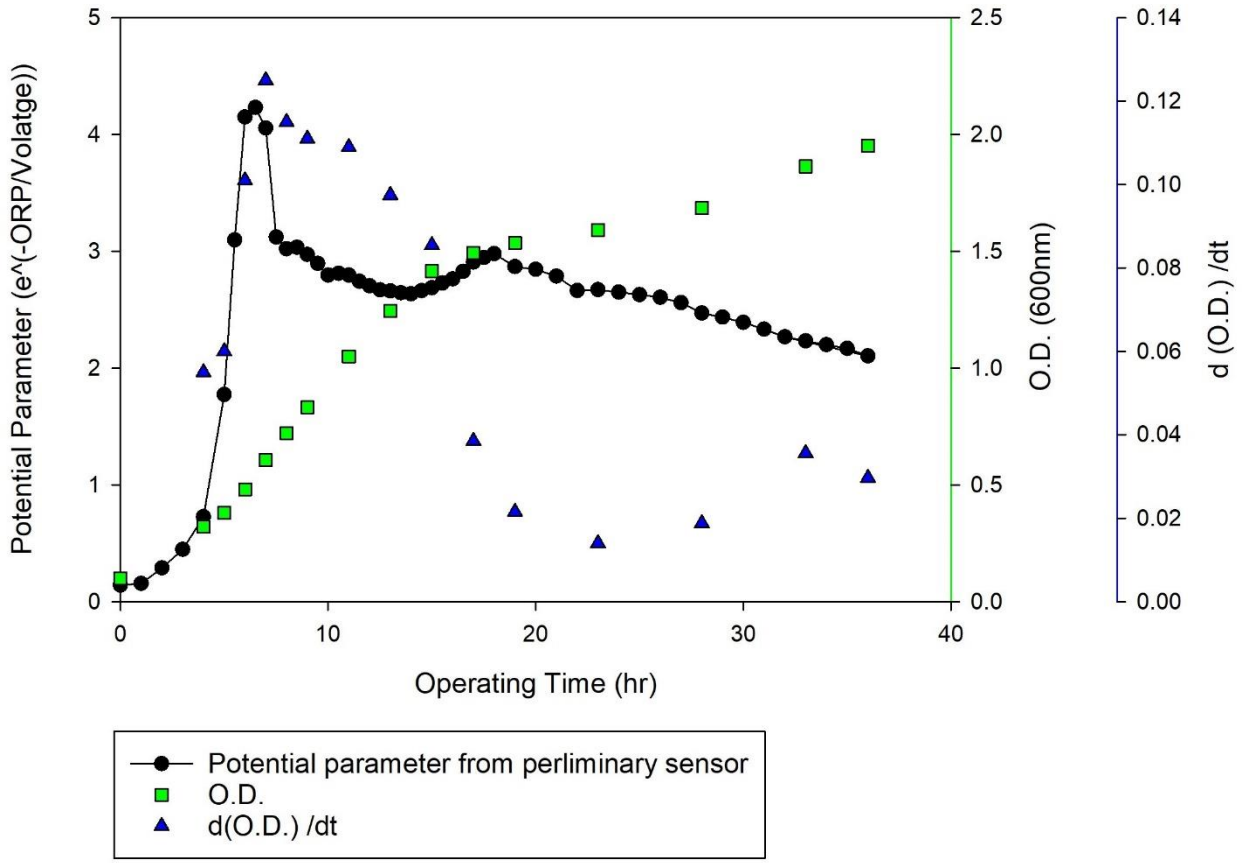

FIGURE 4.1 Potential parameter, OD, and dOD/dt profiles with the preliminary sensor.

4.2 Monitoring microbial growth with the 3D-printed sensor

Similar to the preliminary sensor testing, *B. subtilis* was in the lag phase for the first 5 hours (Figure 4.2). From 0 to 5 hours, the derivative OD value increased by 0.04/hr.

After 6 hours, the derivative OD value showed a noticeable increase to 0.09/hr, indicating bacterial growth had entered the exponential phase.

The 3D-printed sensor's first peak appeared after 10 hours, with the highest potential parameter of 4.06 and the highest derivative OD of 0.18/hr, indicating that starting *B. subtilis* entered a fast growth period after 10 hours. Compared to the preliminary sensor's results, the time required for *B. subtilis* to enter the fast growth stage was longer, which might be due to the different geometric configurations of the preliminary and 3D-printed sensors. Their different sizes and shapes might seriously affect microbial growth and activity. Therefore, the different growth period for *B. subtilis* under the preliminary and 3D-printed sensor can be accepted.

The second peak appeared after 21 hours, and the reaction remained in the stationary phase until the end of the experiment.

The detail microbial growth characteristics for 3D-printed sensor did not display very well (Figure 4.2), potentially due to a deficiency in the design of the 3D-printed sensor. Once in the fast growth phase, the biomass can release a significant quantity of electrons. However, the 3D-printed MFC sensor has a smaller PEM active area and a deeper cathode electrode location than the preliminary MFC sensor, potentially causing slower consumption. After the first peak, the drop in the potential parameter should be sharper since many electrons are transformed into voltage. However, the 3D-printed sensor's slow electron consumption can cause a low voltage output per hour. Furthermore, the many remaining electrons in the medium still need to be consumed even at the late exponential period, which can cause an indistinct second peak. The new 3D-printed sensor's configuration must be accounted for in future studies.

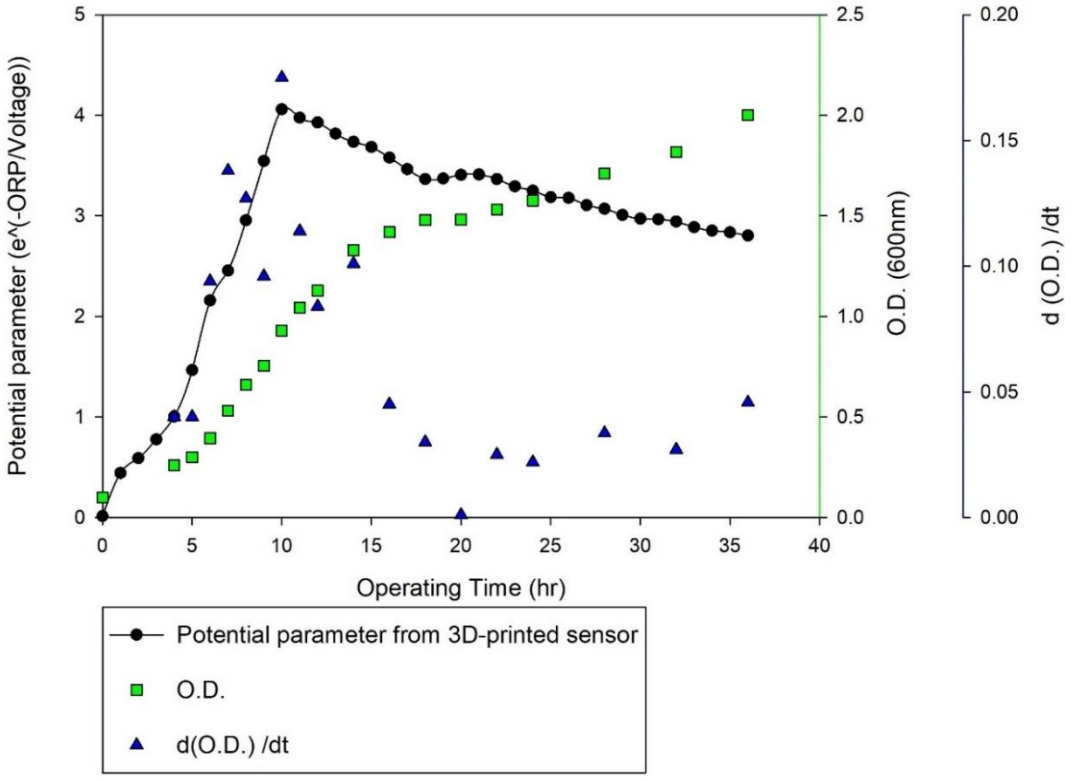

FIGURE 4.2 Potential parameter, OD, and dOD/dt profiles with the 3D-printed sensor.

5 CONCLUSIONS AND RECOMMENDATION FOR FUTURE WORK

Gathering as much information as possible from microbial growth in the soil can significantly increase soil bioremediation utilization. Microbial growth can directly reflect the efficiency of soil bioremediation techniques, and a suitable soil bioremediation technique can be determined. We have previously shown that by integrating MFC and ORP sensors, some detailed microbial growth characteristics could be instantly determined (Shen, 2022). This project's main objective was to minimize the size of MFC and ORP-based sensors for in situ bioremediation applications. Preliminary and 3D-printed sensors were designed and built to achieve a smaller size. Like in the previous experiment (Shen, 2022), two peaks were detected by the preliminary (at 6.5 and 18 hours) and 3D-printed sensors (at 10 and 21 hours), which were supported by accompanying derivative OD values. This novel sensor can monitor microbial growth in real-time, provide detailed growth characteristics in soil, and help select better bioremediation solutions. Additionally, a more responsive 3D-printed sensor will likely be designed in future work to improve its performance and commercial value.

- The 3D-printed sensor should be made cylindrical to minimize the influence of different sensor configurations (cuboidal and cylindrical).
- Based on the cylindrical 3D-printed sensor, the PEM area should be large enough to support protons transfer.
- The new 3D-printed sensor should be shorter to let air fully exchange with the cathode electrode.
- After testing its workability, the 3D-printed sensor's size should be further reduced to minimize costs.

REFERENCE

Aelterman, P., Freguia, S., Keller, J., Verstraete, W., & Rabaey, K. (2008). The anode potential regulates bacterial activity in microbial fuel cells. *Applied Microbiology and Biotechnology*, *78*(3), 409–418.

Aiyer, K. S. (2020). How does electron transfer occur in microbial fuel cells? *World Journal of Microbiology and Biotechnology*, 36(2), 1–9.

Alberghina, F. A. M., & Guarnieri, D. (1975). Change of the cytochrome oxidase level during exponential growth in *Neurospora crassa*. *Experientia*, 31(8), 914–915.

Antoniou, K., & Frank, J. F. (2005). Removal of *Pseudomonas putida* biofilm and associated extracellular polymeric substances from stainless steel by alkali cleaning. *Journal of Food Protection*, *68*(2), 277–281.

Ashraf, M. A., Maah, M. J., & Yusoff, I. (2014). Soil contamination, risk assessment, and remediation. *Environmental Risk Assessment of Soil Contamination*, 1, 3–56.

Beecroft, N. (2010). *Development of a microbial fuel cell (MFC) and analysis of microbial community dynamics*. University of Surrey (United Kingdom).

Beegle, J., & Borole, A. (2018). Exoelectrogens for microbial fuel cells. *Progress and Recent Trends in Microbial Fuel Cells*, 193–230.

Bhargavi, G., Venu, V., & Renganathan, S. (2018). Microbial fuel cells: recent developments in design and materials. *In IOP Conference Series: Materials Science and Engineering* (Vol. 330, No. 1, p. 012034). IOP Publishing.

Bhunia, P., & Dutta, K. (2018). Biochemistry and electrochemistry at the electrodes of microbial fuel cells. *Progress and Recent Trends in Microbial Fuel Cells*, 327–345.

Boas, J. V., Oliveira, V. B., Marcon, L. R. C., Simões, M., & Pinto, A. M. F. R. (2019). Optimization of a single chamber microbial fuel cell using *Lactobacillus pentosus*: influence of design and operating parameters. *Science of the Total Environment*, *648*, 263–270.

Bond, D. R., & Lovley, D. R. (2003). Electricity production by *Geobacter sulfurreducens* attached to electrodes. *Applied and Environmental Microbiology*, *69*(3), 1548–1555.

Brundage, R. (2021, July 9). *The basics of oxidation-reduction potential (ORP)*. pHionics. Retrieved December 14, 2022, from https://www.phionics.com/2021/03/11/the-basics-of-oxidation-reduction-potential.

Chatterjee, P., Ghangrekar, M. M., & Leech, D. (2018). A brief review of recent advances in air-cathode microbial fuel cells. *Environmental Engineering and Management Journal (EEMJ)*, *17*(7).

Chaudhuri, S. K., & Lovley, D. R. (2003). Electricity generation by direct oxidation of glucose in mediatorless microbial fuel cells. *Nature Biotechnology*, *21*(10), 1229–1232.

Chen, L., Cao, C., Wang, S., Varcoe, J. R., Slade, R. C. T., Avignone-Rossa, C., & Zhao, F. (2019). Electron communication of *Bacillus subtilis* in harsh environments. *IScience*, *12*, 260–269.

Copeland, A., & Lytle, D. A. (2014). Measuring the oxidation-reduction potential of important oxidants in drinking water. *Journal of the American Water Works Association*, *106*(1), E10–E20.

Crofts, A. (1996). *Redox potentials*. Redox Potentiometry. Retrieved December 14, 2022, from https://www.life.illinois.edu/crofts/bioph354/redox.html

De Graef, M. R., Alexeeva, S., Snoep, J. L., & Teixeira de Mattos, M. J. (1999). The steady-state internal redox state (NADH/NAD) reflects the external redox state and is correlated with catabolic adaptation in *Escherichia coli*. *Journal of Bacteriology*, *181*(8), 2351–2357.

Dennison, M. J., & Turner, A. P. (1995). Biosensors for environmental monitoring. *Biotechnology Advances*, *13*(1), 1–12.

Di Lorenzo, M., Curtis, T. P., Head, I. M., & Scott, K. (2009). A single-chamber microbial fuel cell as a biosensor for wastewaters. *Water Research*, *43*(13), 3145–3154.

Du, Z., Li, H., & Gu, T. (2007). A state of the art review on microbial fuel cells: a promising technology for wastewater treatment and bioenergy. *Biotechnology Advances*, *25*(5), 464–482.

Dutta, K., & Kundu, P. (2018). Introduction to microbial fuel cells. *Progress and Recent Trends in Microbial Fuel Cells*, 1–6.

El Mekawy, A., Hegab, H. M., Pant, D., & Saint, C. P. (2018). Bio-analytical applications of microbial fuel cell-based biosensors for onsite water quality monitoring. *Journal of Applied Microbiology*, *124*(1), 302–313.

Fiedler, S., Vepraskas, M. J., & Richardson, J. L. (2007). Soil redox potential: importance, field measurements, and observations. *Advances in Agronomy*, *94*, 1–54.

Flimban, S. G., Ismail, I. M., Kim, T., & Oh, S. E. (2019). Overview of recent advancements in the microbial fuel cell from fundamentals to applications: Design, major elements, and scalability. *Energies*, 12(17), 3390.

Foyer, C. H., & Noctor, G. (2005). Redox homeostasis and antioxidant signaling: a metabolic interface between stress perception and physiological responses. *The Plant Cell*, 17(7), 1866–1875.

Gauvry, E., Mathot, A.-G., Couvert, O., Leguérinel, I., & Coroller, L. (2021). Effects of temperature, pH and water activity on the growth and the sporulation abilities of *Bacillus subtilis* BSB1. *International Journal of Food Microbiology*, 337, 108915.

Ghasemi, M., Daud, W. R. W., Ismail, M., Rahimnejad, M., Ismail, A. F., Leong, J. X., Miskan M. & Ben Liew M. (2013). Effect of pretreatment and biofouling of proton exchange membrane on microbial fuel cell performance. *International Journal of Hydrogen Energy*, *38*(13), 5480–5484.

Ghasemi, M., Halakoo, E., Sedighi, M., Alam, J., & Sadeqzadeh, M. (2015). Performance comparison of three common proton exchange membranes for sustainable bioenergy production in a microbial fuel cell. *Procedia Cirp*, *26*, 162–166.

Härtig, E., & Jahn, D. (2012). Regulation of the anaerobic metabolism in *Bacillus subtilis*. *Advances in Microbial Physiology*, 195–216.

Hidalgo, D., Tommasi, T., Bocchini, S., Chiolerio, A., Chiodoni, A., Mazzarino, I., & Ruggeri, B. (2016). Surface modification of commercial carbon felt used as an anode for microbial fuel cells. *Energy*, *99*, 193–201.

Ismail, Z. Z., & Jaeel, A. J. (2016). Modelling study of an up-flow microbial fuel cell catalysed with anaerobic aged sludge. *International Journal of Ambient Energy*, *37*(1), 85–93.

Jaishankar, J., & Srivastava, P. (2017). Molecular basis of stationary phase survival and applications. *Frontiers in Microbiology*, *8*, 2000.

James, C. N., Copeland, R. C., & Lytle, D. A. (2004). Relationships between oxidation-reduction potential, oxidant, and pH in drinking water. *AWWA Water Quality Technology Conference, San Antonio, Texas*.

Jin, Y., Luan, Y., Ning, Y. and Wang, L., 2018. Effects and mechanisms of microbial remediation of heavy metals in soil: a critical review. *Applied Sciences*, *8*(8), 1336.

Jones, H. L., Margaritis, A., & Stewart, R. J. (2007). The combined effects of oxygen supply strategy, inoculum size and temperature profile on very-high-gravity beer fermentation by Saccharomyces cerevisiae. *Journal of the Institute of Brewing*, *113*(2), 168–184.

Jumma, S., & Patil, N. (2016). Microbial fuel cell: design and operation. *Review on Microbiology*, 1–8.

Jung, S. P., Kim, E., & Koo, B. (2018). Effects of wire-type and mesh-type anode current collectors on performance and electrochemistry of microbial fuel cells. *Chemosphere*, *209*, 542–550.

Jurtshuk P Jr. (1996). Bacterial Metabolism. *Medical Microbiology. 4th edition*. University of Texas Medical Branch at Galveston. Chapter 4.

Justino, C., Duarte, A., & Rocha-Santos, T. (2017). Recent progress in biosensors for environmental monitoring: a review. *Sensors*, *17*(12), 2918.

Kalathil, S., Patil, S. A., & Pant, D. (2018). Microbial fuel cells: electrode materials. *Encyclopedia of Interfacial Chemistry*, 309–318.

Karmakar, S., Kundu, K., & Kundu, S. (2010). Design and development of microbial fuel cells. *Current research technology and development topics in applied microbiology and microbial biotechnology. Microbiology Book Series.* Spain: Formatex, *2*, 1029–1034.

Keren, I., Kaldalu, N., Spoering, A., Wang, Y., & Lewis, K. (2004). Persister cells and tolerance to antimicrobials. *FEMS Microbiology Letters*, *230*(1), 13–18.

Khera, J., & Chandra, A. (2012). Microbial fuel cells: recent trends. *Proceedings of the National Academy of Sciences, India Section A: Physical Sciences*, *82*(1), 31–41.

Khilari, S., & Pradhan, D. (2018). Role of cathode catalyst in a microbial fuel cell. *In Microbial Fuel Cell* (pp. 141–163). Springer, Cham.

Ki, D., Popat, S. C., & Torres, C. I. (2016). Reduced overpotentials in microbial electrolysis cells through improved design, operation, and electrochemical characterization. *Chemical Engineering Journal*, *287*, 181–188.

Kruse, P. (2018). Review on water quality sensors. *Journal of Physics D: Applied Physics*, *51*(20), 203002.

Kumar, R., Singh, L., & Zularisam, A. W. (2016). Exoelectrogens: recent advances in molecular drivers involved in extracellular electron transfer and strategies used to improve it for microbial fuel cell applications. *Renewable and Sustainable Energy Reviews*, *56*, 1322–1336.

Kumar, R., Singh, L., & Zularisam, A. W. (2017). Microbial fuel cells: types and applications. In *Waste Biomass Management–A Holistic Approach* (pp. 367–384). Springer, Cham.

Kumar, R., Singh, L., Wahid, Z. A., & Din, M. F. M. (2015). Exoelectrogens in microbial fuel cells toward bioelectricity generation: a review. *International Journal of Energy Research*, *39*(8), 1048–1067.

Kuwertz, R., Martinez, I. G., Vidaković-Koch, T., Sundmacher, K., Turek, T., & Kunz, U. (2016). Material development and process optimization for gas-phase hydrogen chloride electrolysis with oxygen depolarized cathode. *Journal of Applied Electrochemistry*, *46*(7), 755–767.

Li, T., Li, R., & Zhou, Q. (2021). The application and progress of bioelectrochemical systems (BESs) in soil remediation: a review. *Green Energy and Environment*, *6*(1), 50–65.

Li, X., Wang, X., Weng, L., Zhou, Q., & Li, Y. (2017). Microbial fuel cells for organic-contaminated soil remedial applications: a review. *Energy Technology*, *5*(8), 1156–1164.

Liu, C. G., Qin, J. C., & Lin, Y. H. (2017). Fermentation and redox potential. *Fermentation Processes*, 23–42.

Liu, C. G., Xue, C., Lin, Y. H., & Bai, F. W. (2012). Redox potential control and applications in microaerobic and anaerobic fermentations. *Biotechnology Advances*, *31*(2), 257–265.

Logan, B. E., Hamelers, B., Rozendal, R., Schröder, U., Keller, J., Freguia, S., Aelterman, P., Verstraete, W. & Rabaey, K. (2006). Microbial fuel cells: methodology and technology. *Environmental Science and Technology*, *40*(17), 5181–5192.

Lu, Z., Guo, W., & Liu, C. (2018). Isolation, identification, and characterization of novel *Bacillus subtilis*. *Journal of Veterinary Medical Science*, 16-0572.

Mahadevan, A., Gunawardena, D. A., & Fernando, S. (2014). Biochemical and electrochemical perspectives of the anode of a microbial fuel cell. In *Technology and Application of Microbial Fuel Cells*.

Min, B., & Logan, B. E. (2004). Continuous electricity generation from domestic wastewater and organic substrates in a flat plate microbial fuel cell. *Environmental Science and Technology*, *38*(21), 5809–5814.

Mustakeem, M. (2015). Electrode materials for microbial fuel cells: nanomaterial approach. 4(4).

Najafpour, G. (2007). Growth Kinetics. *Biochemical Engineering and Biotechnology*, 81–141.

Needham, J., & Needham, D. M. (1926). The oxidation-reduction potential of protoplasm: a review. *Protoplasma*, *1*(1), 255–294.

Oguz Koroglu, E., Civelek Yoruklu, H., Demir, A., & Ozkaya, B. (2019). Scale-up and commercialization issues of the MFCs. *Microbial Electrochemical Technology*, 565–583.

Oh, S., Min, B., & Logan, B. E. (2004). Cathode performance as a factor in electricity generation in microbial fuel cells. *Environmental Science and Technology*, *38*(18), 4900–4904.

Patel, N., Khan, M. D., Shahane, S., Rai, D., Chauhan, D., Kant, C., & Chaudhary, V. K. (2020). Emerging pollutants in the aquatic environment: source, effect, and challenges in biomonitoring and bioremediation-a review. *Pollution*, *6*(1), 99–113.

Permana, R., Ihsan, Y. N., Riyantini, I., & Agung, M. U. K. (2020). Comparative study between single-chamber and dual-chamber microbial fuel cell on petroleum hydrocarbon degradation in contaminated sediment. *Applied Journal of Environmental Engineering Science*, *6*(2), 6–2.

Piggot, P. J. (2009). *Bacillus Subtilis*. *Encyclopedia of Microbiology*, 3rd ed., Academic Press, Philadelphia.

Pinto, D. (2016). Electronic transfer within a microbial fuel cell. In *Better understanding of Experimental and Structural Parameters at the Interface between Electroactive Bacteria and Carbon-based Electrodes*. Université Pierre et Marie Curie-Paris VI (France), 32-33.

Rahimnejad, M., Adhami, A., Darvari, S., Zirepour, A., & Oh, S. E. (2015). Microbial fuel cell as new technology for bioelectricity generation: a review. *Alexandria Engineering Journal*, *54*(3), 745–756.

Rahimnejad, M., Ghoreyshi, A. A., Najafpour, G. D., Younesi, H., & Shakeri, M. (2012). A novel microbial fuel cell stack for continuous production of clean energy. *International Journal of Hydrogen Energy*, *37*(7), 5992–6000.

Rushdy, A. A., & Othman, A. S. (2011). Bactericidal efficacy of some commercial disinfectants on biofilm on stainless steel surfaces of food equipment. *Annals of Microbiology*, *61*(3), 545–552.

Santoro, C., Arbizzani, C., Erable, B., & Ieropoulos, I. (2017). Microbial fuel cells: from fundamentals to applications. A review. *Journal of Power Sources*, *356*, 225–244.

Saravanan, N., & Karthikeyan, M. (2017). Study of single chamber and double chamber efficiency and losses of wastewater treatment. *International Research Journal of Engineering and Technology*, *5*(3), 1225–1229.

Schröder, U. (2007). Anodic electron transfer mechanisms in microbial fuel cells and their energy efficiency. *Physical Chemistry Chemical Physics*, *9*(21), 2619–2629.

Shen, S. (2022). *Microbial fuel cell-based biosensor for redox potential detection in fermentation process.* University of Saskatchewan (Canada).

Shukla, A., Srivastava, S. and D'Souza, S. (2018). An integrative approach toward biosensing and bioremediation of metals and metalloids. *International Journal of Environmental Science and Technology*, *15*(12), 2701–2712.

Singh, D., Pratap, D., Baranwal, Y., Kumar, B., & Chaudhary, K. (2010). Microbial fuel cells: a green technology for power generation. *Annals of Biological Research*, *1*(3), 128–138.

Slate, A. J., Whitehead, K. A., Brownson, D. A., & Banks, C. E. (2019). Microbial fuel cells: an overview of current technology. *Renewable and Sustainable Energy Reviews*, *101*, 60–81.

Sood, S., Singhal, R., Bhat, S., & Kumar, A. (2011). Inoculum preparation. *Comprehensive Biotechnology*, 151–164.

Steininger, J. M., Pareja, C., & Tech, E. (1996). ORP sensor response in chlorinated water. In *NSPI Water Chemistry Symposium, Phoenix* (Vol. 1).

Tamboli, E., & Eswari, J. (2019). Microbial fuel cell configurations. *Microbial Electrochemical Technology*, 407–435.

Tharali, A. D., Sain, N., & Osborne, W. J. (2016). Microbial fuel cells in bioelectricity production. *Frontiers in Life Science*, *9*(4), 252–266.

Vishwakarma, G., Bhattacharjee, G., Gohil, N. and Singh, V., 2020. Current status, challenges and future of bioremediation. *Bioremediation of Pollutants*, 403–415.

Van Straalen, N. M. (2002). Assessment of soil contamination–a functional perspective. *Biodegradation*, *13*(1), 41-52.

Vlamakis, H., Chai, Y., Beauregard, P., Losick, R., & Kolter, R. (2013). Sticking together: building a biofilm the Bacillus subtilis way. *Nature Reviews Microbiology*, *11*(3), 157–168.

Wang, H. Y., Bernarda, A., Huang, C. Y., Lee, D. J., & Chang, J. S. (2011). Micro-sized microbial fuel cell: a mini-review. *Bioresource Technology*, *102*(1), 235–243.

Xue, X., Bock, C., Birry, L., & MacDougall, B. R. (2011). The influence of Pt loading, support and Nafion content on the performance of direct methanol fuel cells: examined on the example of the cathode. *Fuel Cells*, *11*(2), 286–300.

Yang, W., Li, J., Fu, Q., Zhang, L., Wei, Z., Liao, Q., & Zhu, X. (2021). Minimizing mass transfer losses in microbial fuel cells: theories, progresses and prospectives. *Renewable and Sustainable Energy Reviews*, *136*, 110460.

Yokogawa (2014). *Back to the pHuture: pH and ORP Learning Handbook.* Vigilant Plant. Retrieved December 14, 2022, from https://web-material3.yokogawa.com/TI12B00A20-01E_3.pdf

Zhao, T., & Xu, C. (2009). Fuel cells–Direct alcohol fuel cells | Direct methanol fuel cell: overview performance and operational conditions. *Encyclopedia of Electrochemical Power Sources*, 381–389.

Zhi, W., Ge, Z., He, Z., & Zhang, H. (2014). Methods for understanding microbial community structures and functions in microbial fuel cells: a review. *Bioresource Technology*, *171*, 461–468.

Zhou, T., Han, H., Liu, P., Xiong, J., Tian, F., & Li, X. (2017). Microbial fuels cell-based biosensor for toxicity detection: a review. *Sensors*, *17*(10), 2230.

APPENDICES

Appendix A: Comparison Between Conventional and Novel Portable Biosensors

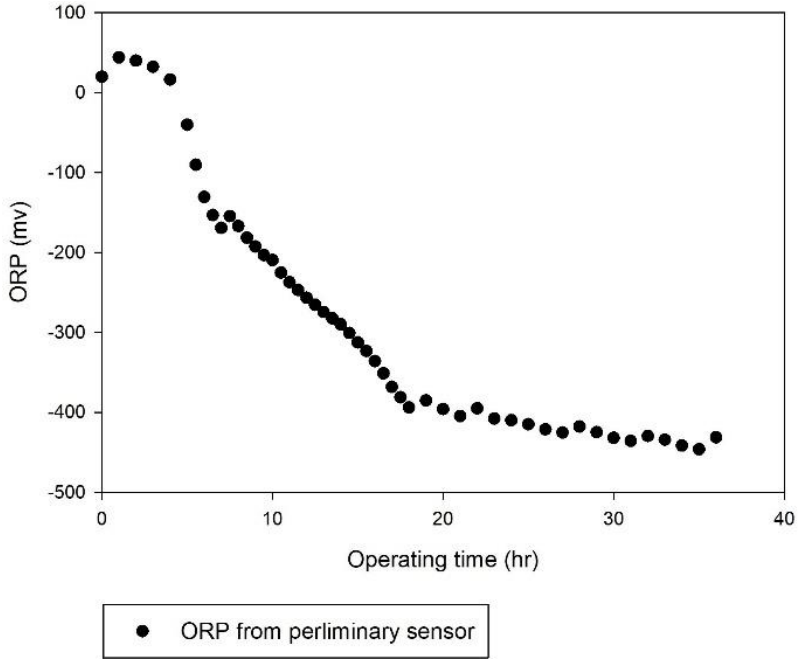

FIGURE A1 ORP biosensor redox potential values through time.

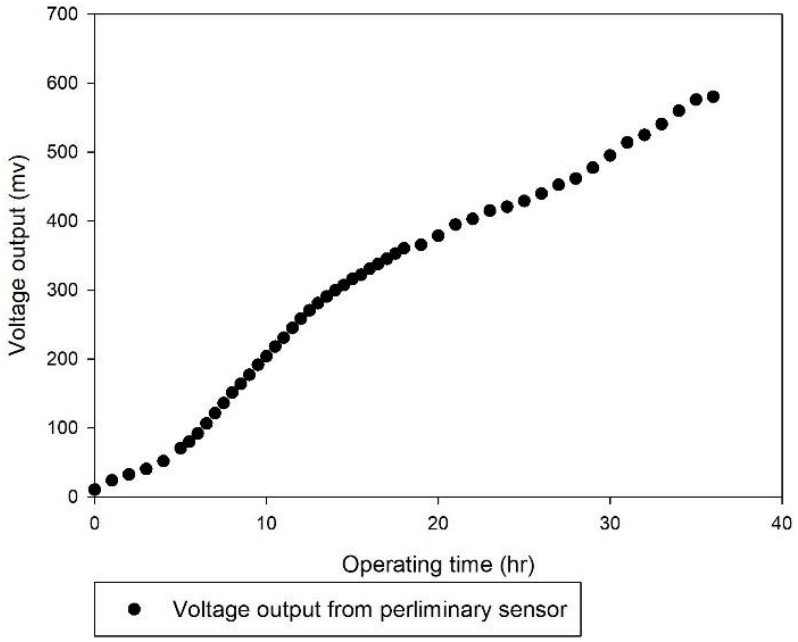

FIGURE A2 MFC biosensor voltage output values through time.

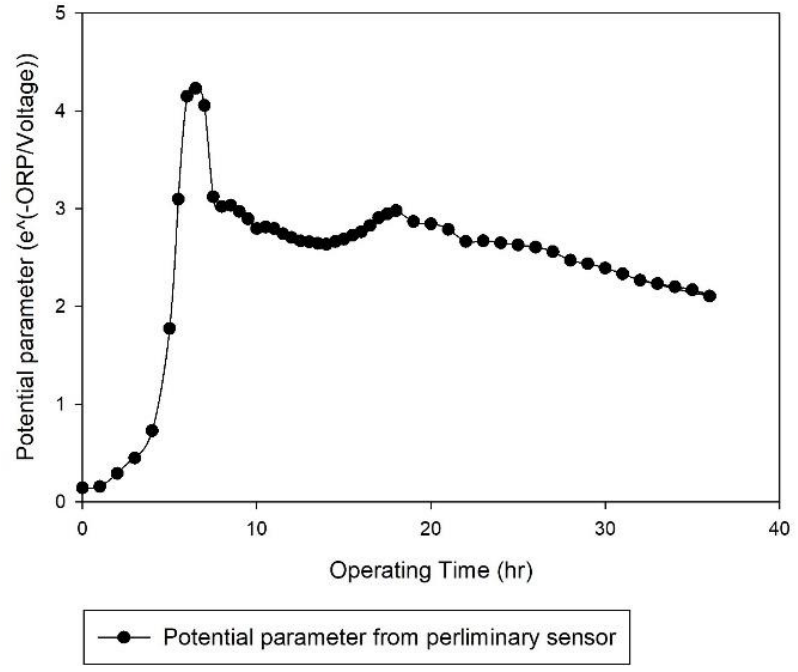

FIGURE A3 The novel portable biosensor's potential parameter values through time.

Appendix B: Proton Exchange Membrane (Nafion 117) Properties

Properties of Nafion® PFSA Membrane

A. Thickness and Basis Weight Properties[1]

Membrane Type	Typical Thickness (microns)	Basis Weight (g/m^2)
N 115	127	250
N 117	183	360
N 1110	254	500

B. Physical and Other Properties[2]

Property	Typical Value	Test Method
Physical Properties		
Tensile Modulus, MPa (kpsi)		
50% RH, 23 °C	249 (36)	ASTM D 882
water soaked, 23 °C	114 (16)	ASTM D 882
water soaked, 100 °C	64 (9.4)	ASTM D 882
Tensile Strength, maximum, MPa (kpsi)		
50% RH, 23 °C	43 (6.2) in MD, 32 (4.6) in TD	ASTM D 882
water soaked, 23 °C	34 (4.9) in MD, 26 (3.8) in TD	ASTM D 882
water soaked, 100 °C	25 (3.6) in MD, 24 (3.5) in TD	ASTM D 882
Elongation at Break, %		
50% RH, 23 °C	225 in MD, 310 in TD	ASTM D 882
water soaked, 23 °C	200 in MD, 275 in TD	ASTM D 882
water soaked, 100 °C	180 in MD, 240 in TD	ASTM D 882
Tear Resistance - Initial, g/mm		
50% RH, 23 °C	6000 in MD, TD	ASTM D 1004
water soaked, 23 °C	3500 in MD, TD	ASTM D 1004
water soaked, 100 °C	3000 in MD, TD	ASTM D 1004
Tear Resistance[3] - Propagating, g/mm		
50% RH, 23 °C	>100 in MD, >150 in TD	ASTM D 1922
water soaked, 23 °C	92 in MD, 104 in TD	ASTM D 1922
water soaked, 100 °C	74 in MD, 85 in TD	ASTM D 1922
Specific Gravity	1.98	—
Other Properties		
Conductivity, S/cm	0.10 min	see footnote[4]
Available Acid Capacity, meq/g	0.90 min	see footnote[5]
Total Acid Capacity, meq/g	0.95 to 1.01	see footnote[5]

FIGURE B1 Properties of Nafion membrane types 115, 117, and 1110.

Appendix C: Raw Data

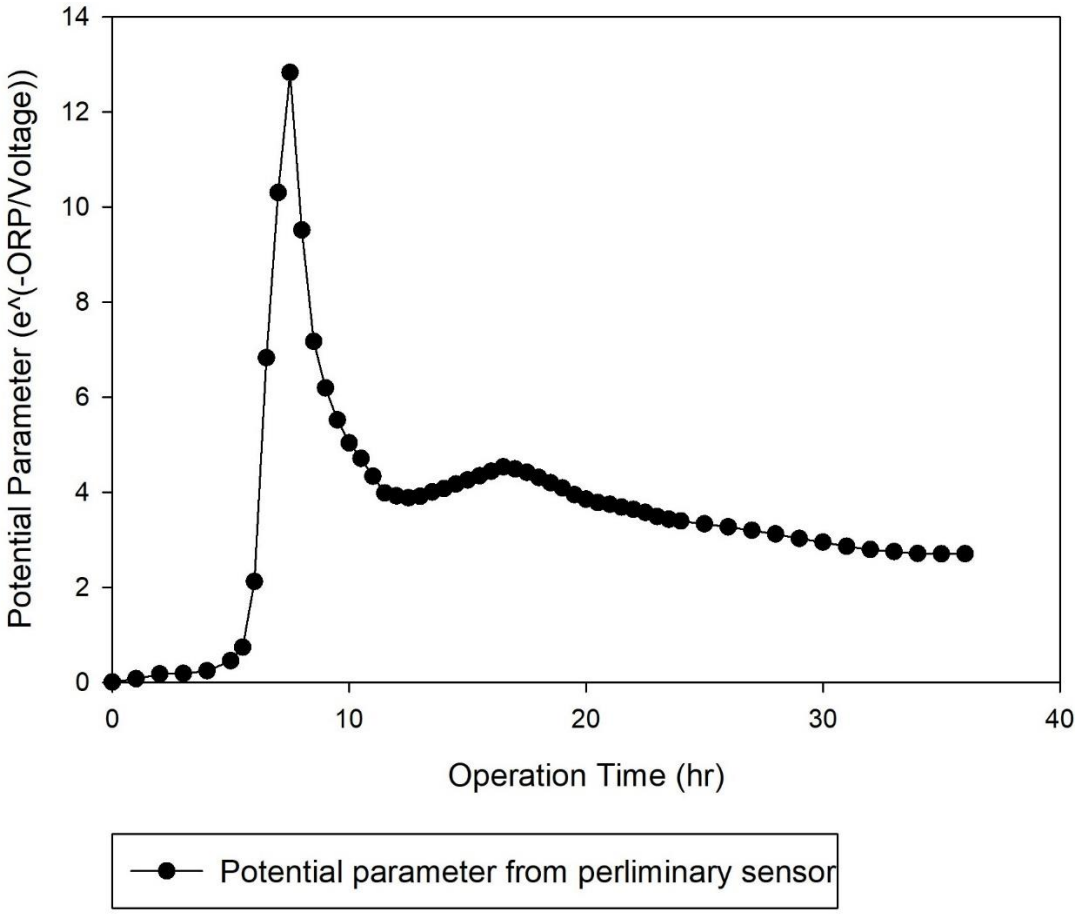

FIGURE C1 The preliminary sensor's potential parameter profile.

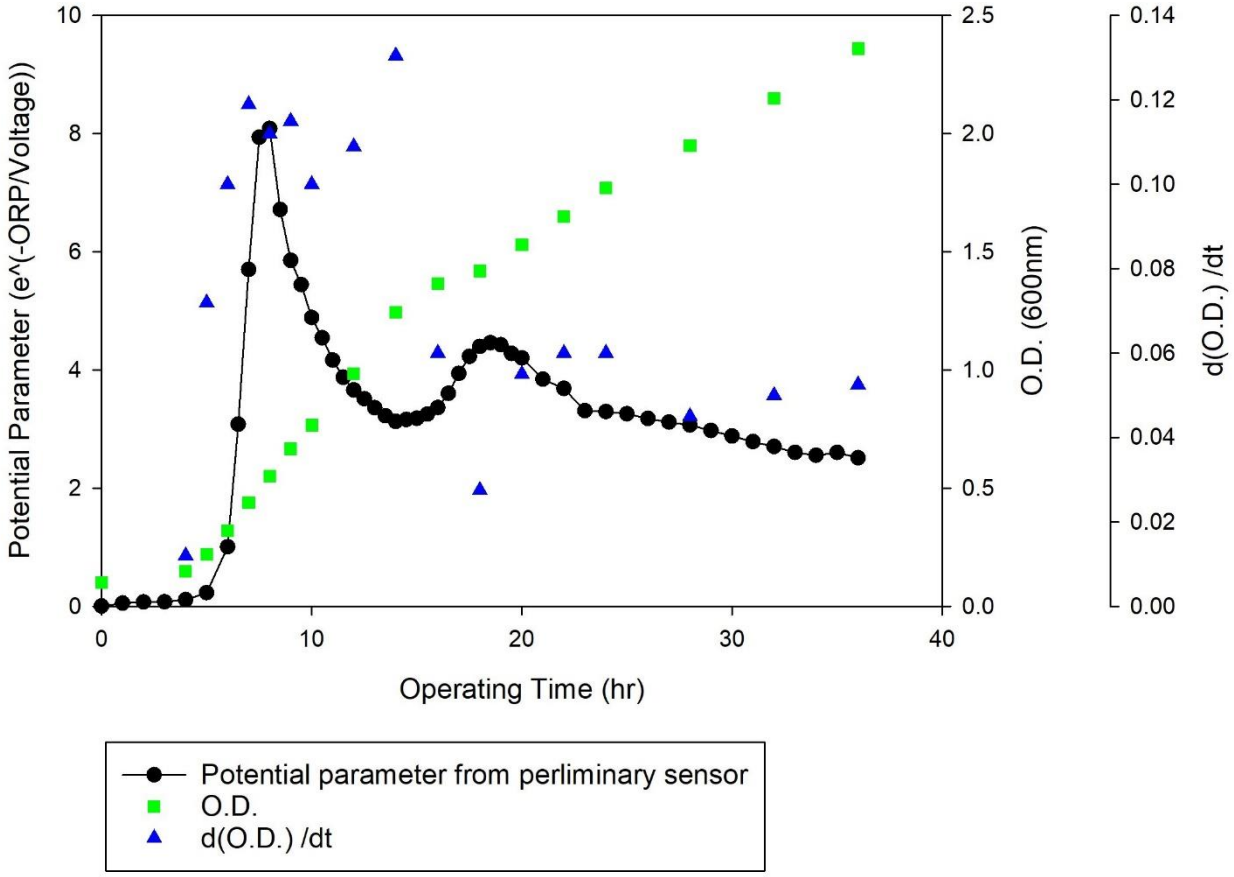

FIGURE C2 The preliminary sensor's potential parameter, OD, and dOD/dt profiles.

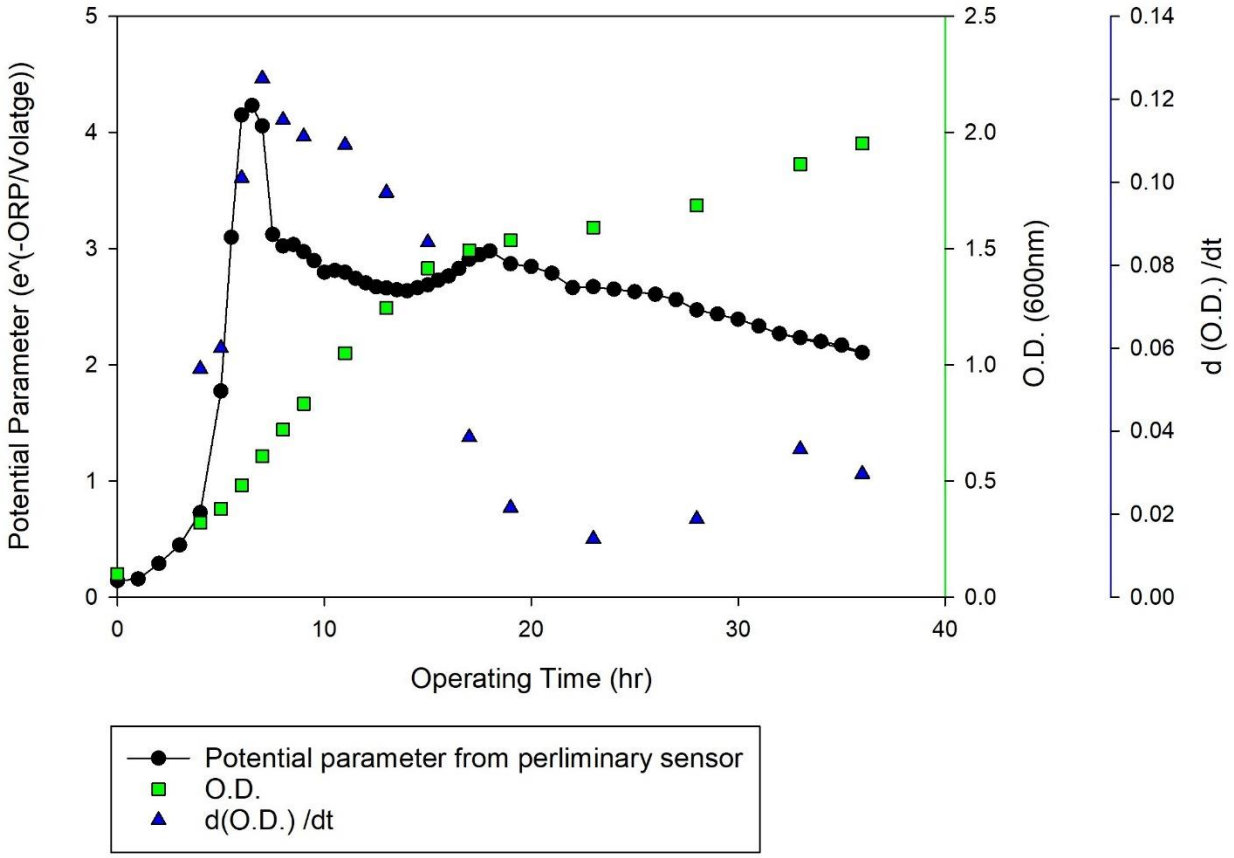

FIGURE C3 The preliminary sensor's potential parameter, OD, and dOD/dt profiles.

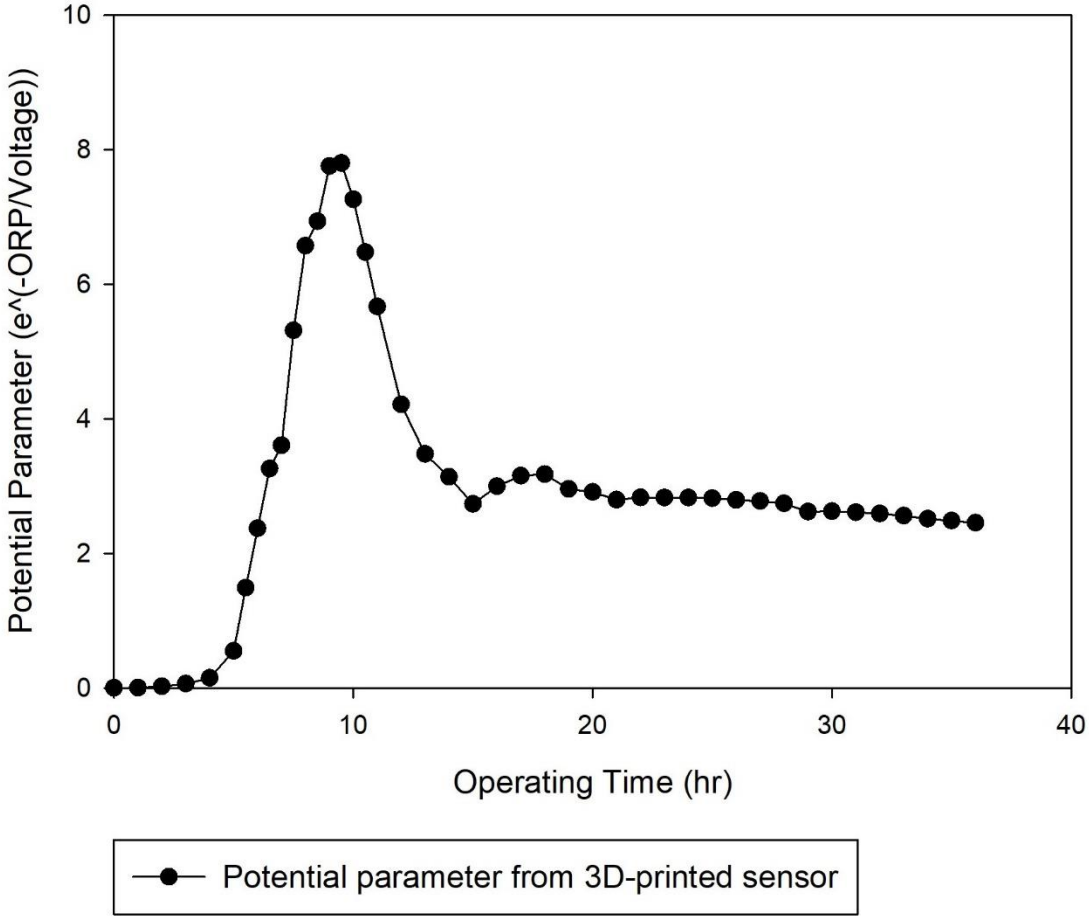

FIGURE C4 The 3D-printed sensor's potential parameter profile.

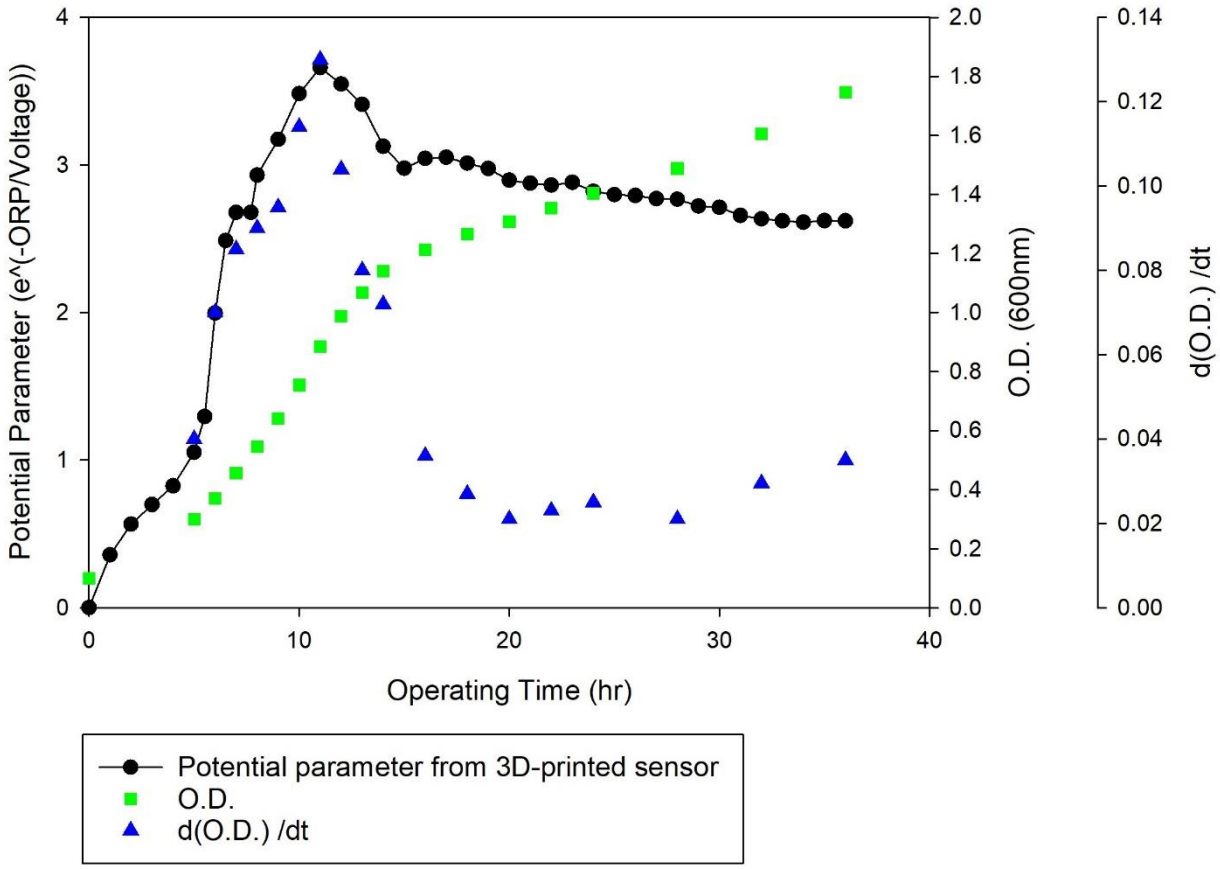

FIGURE C5 The 3D-printed sensor's potential parameter, OD, and dOD/dt profiles.

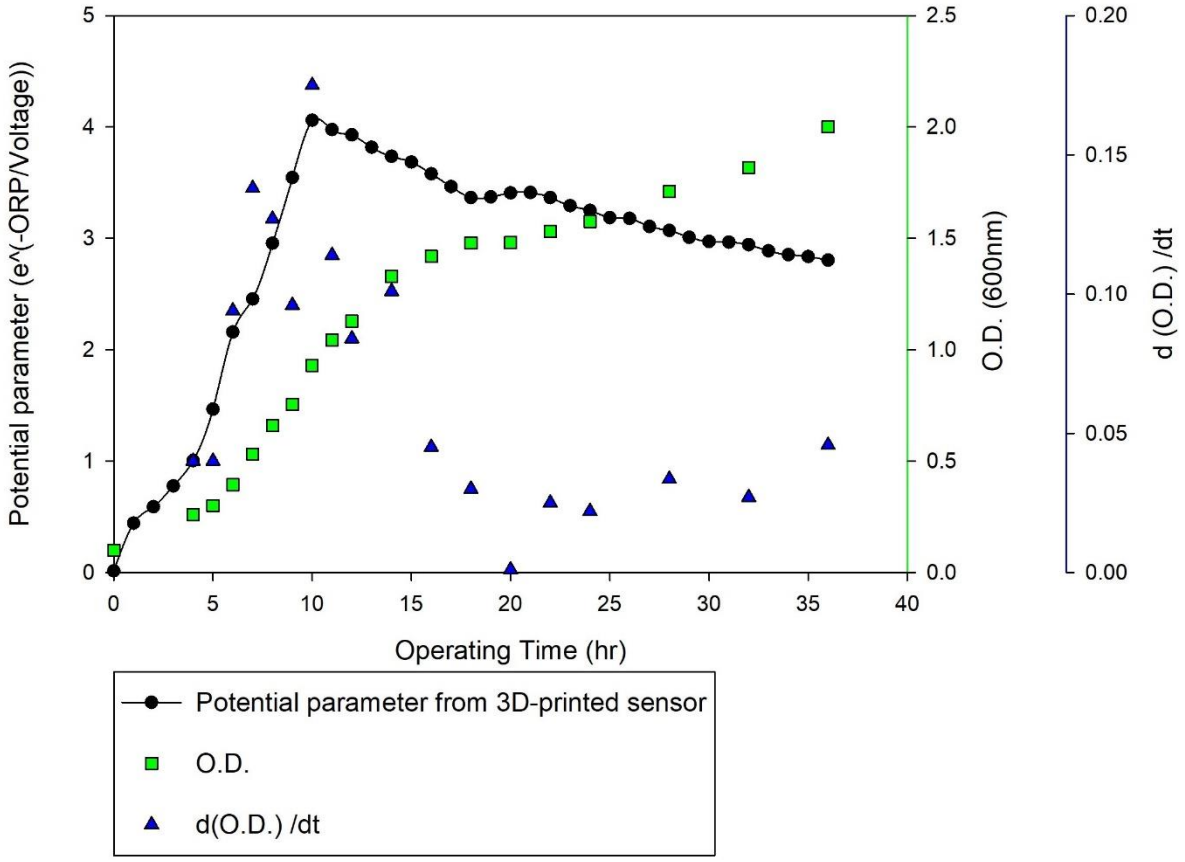

FIGURE C6 The 3D-printed sensor's potential parameter, OD, and dOD/dt profiles.